UNIVERSITÀ DEGLI STUDI DI VERONA

Department of Surgery, Dentistry,

Paediatrics and Gynaecology

Doctoral Programme in Clinical and

Experimental Biomedical Sciences

Cycle/year 34°

Exosomes from human fibroblasts and HaCaT cells cocultured on 3D silk fibroin nonwovens electrospun hybrids stimulate neoangiogenesis and regulate inflammation-related cytokines release

S.S.D. BIO/17

Coordinator: Prof. Giovanni Targher

Tutor: Ass. Prof. Ilaria Pierpaola Dal Prà

Doctoral Student: Dott. Peng Hu

UNIVERSITÀ di VERONA

REGIONE DEL VENETO

The project leading to this application has receivedfunding from the European Union's Horizon 2020 research and innovation programme under the Marie Skłodowska-Curie grant agreement No. 754345, under Region of Veneto Decree nr. 193 of 13/09/2016 and under Università degli Studi di Verona.

INDEX

Abbreviations

3D	Three-dimensional
3D-SFnws	3D silk fibroin nonwovens
3D-SFnws/ES hybrids	3D silk fibroin nonwovens/ electrospun hybrids
ADM	Acellular dermal matrix
AGFs	Angiogenic growth factors
ATR-FTIR	Attenuated total reflectance Fourier transform infrared spectroscopy
bFGF	Basic fibroblast growth factor
CCL	Chemokine (C-C motif) ligand
CXCL	C-X-C motif chemokine ligand
DMEM	Dulbecco-modified Eagle's minimum essential medium
DSC	Differential scanning calorimetry
ECM	Extracellular matrix
ELISA	Enzyme-linked immunosorbent assay
Eotaxin	Eosinophil chemotactic protein
ES	Electrospun / electrospinning
ET	Endothelin

EtO	Ethylene oxide
EVs	Extracellular Vesicles
FBS	Fetal Bovin Serum
GM-CSF	Granulocyte-macrophage colony-stimulating factor
GRO	Growth-regulated oncogene
HDFs	Human dermal fibroblasts
HDMVECs	Human dermal microvascular endothelial cells
HTS	Hypertrophic scar
IFs	Inflammation factors
IL	Interleukin
IP	Interferon γ-induced protein
KGF	Keratinocyte growth factor
LDL	Low-density protein
MVBs	Multi-vesicular bodies
MCP	Monocyte chemoattractant protein
MCP	Monocyte chemoattractant protein
M-CSF	Macrophage colony-stimulating factor
MIP	Macrophage inflammatory protein
MMP	Matrix metallopeptidase

MSCs	Mesenchymal stem cells
NFκB	nuclear factor κ-light-chain-enhancer of activated B cells
PBS	Phosphate-buffered saline
PGA	Polyglycolic acid
PLA	Polylactic acid
SF	Silk fibroin
TGF	Transforming growth factor
Tie-2	Angiopoietin-1 receptor
TIMP	Tissue inhibitor of metalloproteinase
TNF	Tumor necrosis factor
uPAR	Urokinase plasminogen activator surface receptor
VEGF	Vascular endothelial growth factor

Abstract

Background: Silk fibroin (SF), as a natural biomacromolecule, has good biocompatibility, degradability, and potentiality for use as a tissue engineering scaffold material. Previous work suggested that adult human dermal fibroblasts(HDFs) can adhere to a novel type of 3D silk fibroin nonwovens (3D-SFnws) and release exosomes promoting neoangiogenesis. By combining a layer of electrospun SF nanofibers with the original 3D-SFnws scaffolds, we obtained the novel 3D-SFnws/ES hybrid scaffolds. The present study used cocultures of HDFs and human keratinocytes (HaCaT cells) on this new scaffold to assess whether the released exosomes contained factors promoting neoangiogenesis and regulating inflammatory responses.

Method: The features of novel 3D-SFnws/ES hybrids were defined by electron microscopy imaging and specific physical tests. HDFs and HaCaT cells were separately cultured on the opposite sides of this scaffolds and on polystyrene plates using a medium with exosome-depleted FBS. The growth and metabolic activities of the two types of cells on the scaffold were explored by tests assessing DNA amounts and *D*-glucose consumption. The total exosomes were isolated respectively from conditioned media of HDFs and HaCaT cells cocultured on 3D-SFnws/ES hybrids and on Transwell

plates. The exosomes' expression of their specific surface markers CD9 and CD81 was verified using two ELISA kits. Analyses using human cytokines antibody arrays assessed the expression of Inflammation factors (IFs) and Angiogenic growth factors (AGFs) transported by equal quantities of exosomes from the two groups. A tube formation assay was also used to evaluate the exosomes' angiogenic ability by using in vitro cultures of human dermal microvascular endothelial cells (HDMVECs).

Results: Not only the novel 3D-SFnws/ES hybrids imitated the epithelial-mesenchymal structure of normal skin, but also met the typical biomechanical requirements of human soft tissues implants. Compared with experimental day 3, at day experimental 15 in vitro HDFs adhering to the 3D-SFnws side of the new scaffold had increased by 4.7-fold in numbers and metabolized 5.3-fold more *D*-glucose. Also HaCaT cells growing on the scaffold's ES side had increased by 6.5-fold in numbers and metabolized 6.2-fold more *D*-glucose between day 3 and 15 *in vitro*. Exosomes from HDFs and HaCaT cells cocultured on 3D-SFnws/ES hybrids carried significantly higher amounts of IFs than the Transwell group, such as Interleukin-8 (IL-8), IL-10, Monocyte Chemoattractant Protein-1 (MCP-1), Macrophage Inflammatory Protein-1α (MIP-1α), Eosinophil chemotactic protein 2 (Eotaxin-2), Macrophage

Colony-Stimulating Factor (M-CSF), and Tissue Inhibitor of MetalloProteinase-2 (TIMP-2). And the amounts of AGFs, such as Growth-Regulated Oncogene (GRO), Monocyte Chemoattractant Protein-1 (MCP-1), TIMP-1, TIMP-2, and Matrix MetalloPeptidase 9 (MMP-9), were significantly increased in the exosomes isolated from the 3D-SFnws/ES hybrids group. At concentrations from 0.5 to 5 μg/mL, the latter exosomes showed their angiogenic power by inducing HDMVECs to form tubes *in vitro*. However, an alike effect ($P > 0.05$) brought about the exosomes from the Transwell group.

Conclusions: The novel scaffold we obtained by combining a layer of electrospun SF nanofibers with the 3D-SFnws scaffolds not only kept the good physical features of original ones, but also allowed HDFs and HaCaT cells to adhere and proliferate on their opposite sides having different structures. HDFs and HaCaT cells co-grown on these scaffolds released exosomes carrying several AGFs which swiftly induced HDMVECs to form tubes *in vitro*. The same exosomes conveyed IFs capable of promoting and orderly regulating inflammatory response. Thus, we posit that once implanted in vivo this new composite SF scaffold could promote skin wound healing by promoting human keratinocytes and HDFs growth and metabolism, advancing vascularization, and modulating local inflammation.

Key words: Silk fibroin, Nonwovens, Electrospun, Fibroblast, Keratinocyte, HaCaT, Exosome, Angiogenesis, Inflammation, Regeneration, Tissue engineering

Introduction

1. Wound healing and hypertrophic scar

As is well known, the skin is the largest organ of the human body. It is an essential structure that protects internal tissues and organs from UV light, extreme temperatures, mechanical damages, and microbial infections. All of these harming agents can easily injury it. Therefore, one of the goals of researchers and clinicians has been to fully understand the mechanisms operating in wound healing and to find proper therapies to effectively advance wound healing.

Although being continuous and dynamic processes, typically wound healing and skin regeneration can be recapitulated into three overlapping stages: the inflammatory phase; the proliferative phase (entailing cell proliferation and re-epithelization); and the remodeling phase [1]. After an injury, the inflammatory phase is activated at once by the hemostasis and blood coagulation. This phase is marked by the recruitment of the first inflammatory cells, represented by neutrophils, and by the arrival of monocytes and their transformation into macrophages. In the proliferation phase, the core of the healing process lies in the formation of the

granulation tissue, the rebuilding of a vascular network, and covering the wound surface by re-epithelization. In the final remodeling phase, the main progresses are the end of granulation tissue formation and the extracellular matrix (ECM) remodeling whose main components are collagen fibers. A variety of cells and cytokines take part in all the dynamic processes of wound healing, whose most ideal result is the formation of a physiological scar.

However, after severe burns and wounds, the clinical outcome of wound healing is always a disfiguring hypertrophic scar (HTS)., Being common sequelae of cutaneous wound healing, HTSs seriously affect patients' quality of life. Unluckily, effective prevention and treatment methods of HTSs are still lacking, mainly because HTS pathogenesis remains unclear. Its main pathological manifestations are atypical hyperplasia of fibroblasts and excessive deposition of ECM, which result from the interactions of a variety of cells, growth factors, and inflammatory factors. They underlie the human dermal fibrotic diseases [2].

2. Novel biomaterial scaffolds for dermal tissue engineering

When a severe burn or trauma causes a large area of skin loss,

the tradition entails using autologous skin graft transplants. This approach has limits that cannot be ignored, like the availability of a skin source, secondary injury production, and its secondary scar formation caused by invasive skin removal. So, it is essential to cover with dressings the wound surface [3]. With the development of biomaterial science and biomedical engineering, tissue-engineered dermal substitutes have become important devices aimed at repairing skin defects. The ideal dermal substitute should imitate the original structure and function of the skin and should have the following features:

Firstly, the most important prerequisite is good biocompatibility. Other significant characteristics must be the lack of an obvious inflammatory reaction, immune reaction, and cytotoxicity. And it would be better if the substitute adorbs secretions and prevents the occurrence of infections, adhesions, and scar formation [4]. Secondly, there must be a good interface between the biomaterials and tissue cells, which should simulate the ECM of the original skin, and should benefit cell adhesion, spreading, and reproduction. Thirdly, the biomaterial must be easy to process, and should have an ideal three-dimensional (3D) spatial structure at the molecular level. It should maintain its original shape after transplantation, and have a proper biodegradability and degradation rate. In other words,

the degradation and absorption rates both in vitro and after implantation in vivo should match the growth rates of cells and tissues. Last but not least, the biomaterial should provide appropriate 3D sites and cues for the storage and release of cellular growth factors and cell anchoring [5] .

The use of an acellular dermal matrix (ADM) as a natural biomaterial skin scaffold apt to repair tissue defects has been frequent in clinical settings. ADM obtains from allogeneic or xenogeneic skin. It keeps the dermal matrix once chemical methods have removed all its highly immunogenic cellular components. ADM promotes the formation of basement membranes and accelerates the proliferation and differentiation of epidermal cells. The implanted epidermal cells can tightly adhere to the basement membrane surface of ADM, and induce the orderly growth and differentiation of fibroblasts and vascular endothelial cells [6]. At present, excepting autologous skin, allogeneic ADM, such as AlloDerm® approved by FDA, has been widely used in clinical settings as the best skin substitute and has also achieved good results [7, 8]. But the materials come from human fresh cadaver skin. Hence, a series of barring reasons, such as limited resources, high prices, unavoidable religious and ethical problems, have been hindering its large-scale promotion and clinical use.

Thus, xenogeneic ADMs from animals (swine and cattle) have also been developed for clinical wound repairing. Various studies have verified that they can promote wound tissue regeneration and healing in vivo [9, 10]. However, the existence of zoonotic diseases such as swine (e.g. blue ear disease), cattle (e.g. mad cow disease), and the potential risk of transmitting viruses cannot be ignored.

In recent years, some researchers have been interested in the human amniotic membrane, which is a thin film-like placental tissue, containing laminin, collagen, and fibril-binding protein. The cell-free connective tissue left after amniotic membrane decellularization has reasonable mechanical properties and can mitigate immune rejection [11]. Decellularized amniotic membranes not only have the 3D structure required by biological scaffolds but are also endowed with biologically active molecules that promote cell growth. However, various limiting factors, such as finite sources, complex production processes, high production costs, difficulty in industrial scaling up, and the risks of spreading diseases, also prevented the decellularized amniotic membranes from becoming the most promising biomaterial.

The chemical polymers, such as the synthetic potential skin scaffold, are generally inferior to natural materials in terms of

biocompatibility and cellular affinity, but are provided with advantages in terms of controlled biodegradation rate, mechanical properties, processing performances, manufacturing costs, and wide applications range. These materials include polygalactose, nylon mesh, polylactic acid (PLA), and polyglycolic acid (PGA). However, wounds covered with these materials still require second-stage surgical grafting with autologous epidermis. Moreover, their degradation products may be cytotoxic, may induce inflammatory reactions, and may even be susceptible to local infections on the wound surface.

3. Silk fibroin

As a gift from Nature, silk has been used for over two thousand years in human life. Its main constituent, named silk fibroin (SF), is a biomacromolecule obtained from silk fibers through a degumming process and accounts for 70-80% of the silk fiber mass [12]. As a natural biopolymer, SF has good biocompatibility, controllable biodegradability, and in addition relatively low production cost. SF has been selected as the raw material for the tissue engineering scaffold in a variety of tissue engineering studies [13, 14]. Structurally, SF is a stable anti-parallel folded molecule, which

includes two different conformations, Silk Ⅰ and Silk Ⅱ. Moreover, these two conformations are interchangeable according to the different physicochemical conditions. This determines the good mechanical strength of SF in the long-axis direction and its remarkable plasticity [15]. The features proper of SF fully meet the requirements or criteria for its use as a biomedical material [16]: First, as a natural polymeric fibrous protein, SF can be highly purified, which entails a very low risk of transmitting diseases and almost no potential hazards. Second, SF can be chemically modified by different treatments on certain side-chain amino acids to obtain a variety of morphologies. Third, the biological degradation speed of SF is mostly slow and its final degrading products are not harmful. Finally, SF is cheap and easy to prepare from abundant sources. It is important that the SF properties be not changed after high-pressure sterilization, ethylene oxide sterilization, or other sterilization methods. These features make SF a highly suitable candidate for clinical application. SF can be modelled in various conformations via electrospinning, ultrasound, salting out, and freeze-drying technologies employing different physicochemical conditions and modalities of action [17].

The research on SF as an artificial dermal scaffold has been progressing during the last decades and has confirmed SF

potential as a biomaterial scaffold for dermal tissue engineering. Hodgkinson et al. used the electrostatic spinning technique to obtain a structured SF protein-based nanofibrous scaffold. Thus, they proved that the SF scaffold can advance the proliferation and re-epithelization by keratin-synthesizing cells, which suggested that SF scaffolds can promote wound healing [18]. The results of a recent remarkable study with 71 patients based on the randomized single-blind parallel controlled clinical trial proved that, compared to the commercial wound dressings, SF films significantly shortened the wound healing average time while improving skin regeneration and reducing the occurrence of adverse events [19]. What is more gratifying is the notion that that non only the mulberry SF of the domesticated Bombyx mori silkworm but also the non-mulberry SFs from different wild silkworms and spiders can accelerate wound healing presumably by regulating the de novo deposition of ECM [20].

4. Exosomes

Exosomes are membrane-bound extracellular vesicles (EVs) incessantly produced and released into the ECM by somatic cells of any age. Therefore, exosomes can be found in many or even all

kinds of bodily fluids, including blood, urine, cerebrospinal fluid, and in cell culture media too [21]. The diameter of exosomes ranges from 30 to 100 nm. Hence, they are larger than low density proteins (LDLs), but smaller than other kinds of vesicles (e.g. apoptotic bodies) or blood cells. Exosomes are assembled inside the multi-vesicular bodies (MVBs). When mature MVBs fuse with the inner surface of the cell plasma membrane, the exosomes they carry are immediately released into the extracellular environment [22]. According to reports, exosomes convey cytokines, proteins, lipids, mRNAs, microRNAs (miRNAs), non-coding RNAs (ncRNAs), ribosomal RNAs (rRNAs), cytokines, and chemokines [23]. According to accumulating direct evidences, exosomes play a key part in the whole process of blood coagulation, in information transmission between neighboring and far away somatic cells, and in waste management processes [24]. Their roles in the recipient cells include hormone regulation, capillary remodeling, cell proliferation, division, apoptosis, tumor cell metastasis. Thus exosomes help keep human physiological processes, and participate in the processes underlying diseases [25]. Therefore, the interest in the clinical applications of exosomes has been increasing with time because of their potential function as drug/protein delivery carriers.

5. Keratinocyte-fibroblast interactions in wound healing

Different wound-healing phases are now recognized. However, the proliferation and early remodeling stage often determine the quality of the wound healing process, including granulation tissue formation, collagen deposition, epithelial regeneration, early remodeling of ECM, wound contraction, and so on. Stromal cells are mostly activated in the granulation tissue, where they proliferate and synthesize big amounts of ECM. To seal the wound defect, the epithelial cells both proliferate and concurrently migrate onto the temporary ECM synthesized by the granulation tissue. Fibroblasts and keratinocytes, as the main effector stromal cells and effector epithelial cells, respectively, participate in practically all of the aforementioned activities: their reciprocal interactions, represented by paracrine exchanges, have profound effects on this dynamic process. Ample evidence shows that keratinocytes stimulate fibroblasts to generate and release growth factors, which in turn promote keratinocyte proliferation. This is a paracrine process bidirectionally working that is vividly summarized here as "Keratinocyte-Fibroblast Interactions" [26].

At present, there is no clear and indisputable evidence that the

just mentioned paracrine processes are conducted through the bidirectional release and uptake of exosomes. However, the results of researches on cardiovascular diseases, tumors, and labor delivery have proved that exosomes are the mediators of paracrine effects [27-29]. In addition, research using mesenchymal stem cells (MSCs) to promote myocardial cell repair following ischemia-reperfusion damage confirmed that exosomes play paracrine roles [30]. Subsequently, various studies also showed that the exosomes released from many kinds of MSCs do promote wound healing [31, 32].

Previously, we showed that two kinds of 3D silk fibroin nonwovens (3D-SFnws) grafted into the subcutaneous tissue of mice were rapidly vascularized via molecular pathways that were not clarified [33-35]. In a more recent work using a carded-hydroentangled 3D-SFnws, we proved that the exosomes released from adult human dermal fibroblasts (HDFs) grown on this 3D-SFnws conveyed multiple angiogenic/growth factors (AGFs) which induced human dermal microvascular endothelial cells (HDMVECs) to rapidly build up endothelial tubes *in vitro* [36]. It is indisputable that we also need to clarify the keratinocyte-fibroblast interactions during the wound healing process before the novel kind of 3D-SFnws scaffold can be employed in clinical trials.

Very recently, we have further improved the scaffold manufacturing technique by adding a continuous layer of electrospun (ES) SF nanofibers to one side of the carded-hydroentangled 3D-SFnws. Thus we obtained the fourth type of SF scaffold, which is a 3D-SFnws/ES hybrid. Because the new 3D-SFnws/ES hybrids have two differently structured sides, they are fit to set up separated co-cultures of epithelial and mesenchymal cells i.e. keratinocytes on the ES surface and fibroblasts on the 3D-SFnws surface. Thus, the 3D-SFnws/ES hybrids can model the keratinocyte-fibroblast interactions in the process of wound healing. And, keeping also the focus on the exosomes as paracrine mediators, this study was planned to investigate the influence of the keratinocytes/fibroblasts harboring 3D-SFnws/ES hybrids on the process of neoangiogenesis. Moreover, we decided to investigate whether the exosomes released from the keratinocytes and fibroblasts separately co-cultured on the new 3D-SFnws/ES hybrids might impact the regulation of the inflammatory processes involved in wound healing.

Materials and Methods

1. Materials

1.1. Reagents

Table. 1 Reagents used in our experiments

Name	*Source*
Bio-raid protein assay reagent	Bio-Rad (USA)
BSA	Gibco (USA)
DMEM	Gibco (USA)
FBS	Gibco (USA)
PBS	Gibco (USA)
PEN - STREP	CAMBREX (Belgium)
0.25% Trypsin - EDTA	Gibco (USA)
Endothelial Cell Media MV/MV2	PromoCell (Germany)
Vybrant Cell-Labeling Solution	Thermo Fisher (USA)
Total Exosome Isolation	Invitrogen (USA)
Quant-IT dsDNA Reagents and Kits	Invitrogen (USA)
Amplx Red Glucose Oxidase Assay Kit	Invitrogen (USA)
ExoTEST kit for ELISA Exosome quantification	HansaBioMed (Estonia)
ExoELISA - ULTRA Complete Kit (CD81)	SBI Systembio (USA)
C-Series Human Inflammation Antibody Array	RayBiotech (USA)
C-Series Human Angiogenesis Antibody Array	RayBiotech (USA)
DyLight 800-conjugated streptavidin protein	Thermo Fisher (USA)
Angiogenesis Assay Kit (Tube Formatiom)	PromoKine (Germany)

1.2. Cells

Nontumorigenic human dermal fibroblasts (HDFs) were bought from ScienCell Research Laboratories (USA). The supplier company guaranteed, via Cell Applications (USA), that these HDFs expressed fibronectin and were negative for human immune deficiency virus, hepatitis B virus, hepatitis C virus, mycoplasma, bacteria, yeasts and fungi. The standard culture medium for the HDFs was Dulbecco's minimum essential medium (DMEM) (89% v/v; Gibco, USA) fortified with complements heat-inactivated (at 56 °C for 30 minutes) foetal bovine serum (FBS) (10% v/v; Gibico, USA) and penicillin– streptomycin solution (1% v/v; CAMBREX, Belgium). For the specific experiments, the standard FBS was changed to bovine exosome-depleted FBS.

HaCaT cells (NO. 300493) were bought from CLS Cell Lines Service GmbH (Germany). The results of viruses tests conducted by Real-Time PCR were negative. HaCaT cells, which derive from adult human skin, are spontaneously transformed keratinocytes isolated from histologically normal skin samples cultured *in vitro* [37]. The standard culture medium for the HaCaT cells was also Dulbecco's minimum essential medium (DMEM) (89% v/v; Gibco, USA) fortified complements heat-inactivated (at 56 °C for 30 minutes) foetal bovine serum (FBS) (10% v/v; Gibico, USA) and

penicillin–streptomycin solution (1% v/v; CAMBREX, Belgium). The standard FBS was also changed to exosome-depleted FBS for the specific experiments.

Human dermal microvascular endothelial cells (HDMVECs) isolated from adult skin capillaries were bought from Cell Applications (USA). The seller pledged that such cells were free from bacteria, yeasts, fungi, and mycoplasma, and that they expressed the Factor VIII-related antigen. HDMVECs were grown in endothelial cell growth basal medium (PromoCell, Germany) fortified with 10% v/v heat-inactivated FBS. For the tube formation experiments, the standard FBS was changed to exosome-depleted FBS.

1.3. The production of the carded/hydroentangled 3D-SFnws and the preparation of 3D-SFnws/ES hybrids

The 3D-SFnws were produced as previously reported [36]. Briefly, sericin-deprived (via standard de-gumming) spun silk from comber waste in staple form (average fiber length, 50 ± 7 mm) underwent processing in a cotton-type flat carding machine (width, 100 cm). Next, the web formed via carding received a mechanical hydroentanglement on both its surfaces that created several bonding points on it.

The 3D-SFnws/ES hybrid was produced by adding the electrospinning (ES) technology. A layer of ES SF nanofibers was deposited onto one side of the 3D-SFnw mounted on a rotating steel cylinder of 2.5 cm diameter and 25 cm length (the collector). To prepare the electrospinning dope, degummed SF fibers were dissolved for 3 hours in an aqueous solution of 9.3 M lithium bromide at 60 °C. The hybrid composite underwent dialysis against distilled water to remove salts. The aqueous SF solution was cast in Petri plates and baked in a vented oven at 35 °C until complete water evaporation. The thus obtained SF films were dissolved in formic acid at 8% w/v to obtain the ES dope. Electrospinning was performed as previously reported [38], using the following experimental parameters: potential difference = 25 kV; flow rate = 0.8 ml h-1; and spinneret–collector distance = 14 cm. Coupling of the ES layer with the 3D-SFnw was achieved during electrospinning, according to a patented process [39]. A solution of ionic liquid (1-ethyl-3-methylimidazolium acetate; EMIMAc) in water (EMIMAc/water 80/20% v/v) was used as the welding medium.

After electrospinning, the 3D-SFnws/ES hybrid was removed from the collector, flattened, and stabilized by dipping into aqueous ethanol (80 vol%) followed by overnight washing in distilled water and finally drying. The obtained hybrid substrate was further

purified by a microwave-assisted extraction with ethanol to remove processing aids, next dipped into distilled water overnight, dried, packaged under a laminar flow cabinet, and finally sterilized with Ethylene oxide (EtO).

2. Methods

2.1. Tests for the 3D-SFnws/ES hybrids

2.1.1. Scanning electron microscopy (SEM)

To be morphologically analysed, 3D-SFnws/ES hybrids were sputter coated with Au/Pd under a reduced-argon atmosphere in a Desk V Coating System (Denton Vacuum, USA) and observed under the following conditions: 10 kV acceleration voltage; 100 A beam current; and 15 mm working distance in a Zeiss EVO MA10 scanning electron microscope.

2.1.2. Attenuated total reflectance Fourier transform infrared spectroscopy (ATR-FTIR)

An ALPHA Fourier transform infrared spectrometer (Bruker, Italy) equipped with an attenuated total reflectance accessory served to analyze the samples by collecting 65 scans at a 4 cm^{-1} resolution in the infrared 4000 - 400 cm^{-1} wavenumber range. Spectra were corrected with a linear baseline and normalized to the

CH_2 bending peak at about 1445 cm^{-1}, a peak notoriously insensitive to the molecular conformation of SF.

2.1.3. Differential scanning calorimetry (DSC)

The thermal properties of the 3D-SFnws/ES hybrids were determined by a calorimeter (DSC 3500 Sirius, Netzsch, Germany). Samples (3–5 mg) were sealed in aluminium pans and subjected to a heating cycle from 50 ℃ to 400 ℃, at a heating rate of 10 ℃/min, under a sweeping N_2 atmosphere (flow rate of 20 ml/min).

2.2. Cell culture on 3D-SFnws/ES hybrids

2.2.1 Preparation of 3D-SFnws/ES hybrids for in vitro cell cultures

After a thorough washing in phosphate buffer saline (PBS), 3D-SFnws/ES hybrids samples were transversally cut into circular pieces of 35 mm in diameter, sealed in pouches and sterilized at 55 ℃ for 3 hours by exposring them to an EtO/CO_2 (10/90 v/v) mixture under a pressure of 42 psi (≈290kPa) in a vacuum oven. Next, the specimens were degassed for 8 hours at 50 ℃ in a vacuum oven after staying for 24 hours in an aeration room. Prior to use, the sterilized 3D-SFnws/ES hybrids were systematically evaluated by checking for the absence of morphological changes and the maintenance of their mechanical properties.

2.2.2 Preparation of cell culture medium devoid of bovine

exosomes

The experimental growth medium was reinforced with a 10% v/v exosome-depleted FBS to guarantee that the exosomes under research were purely from HDFs and HaCaT cells, with no contamination from FBS-carried exosomes. To do this, the heat-inactivated (at 56 °C for 30 minutes) FBS was spun down twice with the centrifugal force of 100,000 g for 120 minutes in an Optima TLX ultracentrifuge equipped with a TLA 100.3 mini rotor before being added to the cell culture medium (Beckman, USA) [40].

2.3. Intravital HDFs and HaCaT cells staining

1) Prior to use, 3rd or 4th passage HDFs and HaCaT cells were counted using a handheld automated cell counter (Scepter, Merck, Germany) following the manufacturer's instructions.

2) Cells were suspended at a density of 1.0×10^6 in the FBS-free medium (DMEM 99% v/v; Gibco, USA and penicillin– streptomycin solution 1% v/v; CAMBREX, Belgium).

3) Next, 5μL of the cell-labeling solution (Thermo Fisher, USA) was added to each mL of cell suspension followed by mixing via gentle pipetting.

4) The tubes harboring the labeled cell suspension were incubated

for 20 minutes at 37 ◦C and next spun down at 1500 rpm for 5 minutes. Then the supernatant was removed and the cells gently resuspended in a warm culture medium, i.e. DMEM (89% v/v; Gibco, USA), FBS (10% v/v; Gibico, USA), and penicillin-streptomycin solution (1% v/v; CAMBREX, Belgium).

5) Six ready-to-use 3D-SFnws/ES hybrids follow were put into as many sterilized wells inside polystyrene culture plates (with lid, SPL LIFE SCIENCES, South Korea). Sterilized tweezers gently flattened the edges of the samples at the bottom of the wells. Typically, three of the hybrids had the rough 3D-SFnws side up and another three had the smooth ES side up.

6) After counting with a handheld automated cell counter (Scepter, Merck, Germany), the labeled HDFs (1×10^5 for each sample) were seeded onto three rough sides of the 3D-SFnws of each hybrid scaffold. Then 5 ml of culture medium were added to each well. The same procedure was performed for the HaCaT cells, the difference being that the HaCaT cells were seeded onto the smooth ES side of each 3D-SFnws/ES hybrid.

7) The cell cultures of both groups were incubated for 15 days under standard conditions (i.e. 37 ℃, 95% v/v air, 5% v/v CO_2). The cells were regularly observed under an inverted fluorescence microscope (IM35, Zeiss, Germany) fitted with proper excitation

and emission filters. Digital pictures were taken with a C-P12 digital camera (OPTIKA, Italy) at 40× magnification.

2.4. Quant-iT PicoGreen DNA quantifification

To estimate the proliferation of cells grown on 3D-SFnws/ES hybrids, DNA cellular contents were assessed using the Quant-IT PicoGreen double-stranded DNA (dsDNA) Kit (Invitrogen, USA). Three specimens of HDFs cultured on the rough 3D-SFnws side of the hybrid scaffold were sampled at experimental days 3 and 15. After washing the cells in PBS, 2 ml of deionized water was added to each well to detach and lyse the cells. Twice repeated freezing-thawing cycles improved cell lysis. dsDNA amounts were next fluorometrically measured at an excitation λ 480 nm and an emission λ 520 nm. A standard dsDNA curve of known increasing cell numbers was used to calibrate the fluorescence intensities. The same procedure was done for the HaCaT cells, that as mentioned were cultured to the smooth ES side of 3D-SFnws/ES hybrids.

2.5. Assay of D-glucose consumption

D-glucose cumulative consumption by the two types of cultured on 3D-SFnws/ES hybrids was respectively assessed in

correspondingly conditioned growth media samples using a glucose oxidase assay, i.e. the Amplex Red Glucose/Glucose Oxidase Assay Kit (Invitrogen, USA). Three specimens of HDFs were cultured on the rough 3D-SFnws side of the hybrid scaffold (HaCaT cells cultured on the smooth ES side), and every 2 days from experimental days 3 to 15 the cell-conditioned media were collected and changed with fresh ones. Following the seller's directions, the glucose oxidase interacted with D-glucose to produce D-gluconolactone and hydrogen peroxide via horseradish peroxidase. In a 1:1 stoichiometric ratio, hydrogen peroxide combined with the Amplex Red reagent to produce the red fluorescent product Resorufin, the intensity of which was measured fluorometrically at excitation and emission wavelengths of 560 and 590 nm, respectively.

2.6. HDFs and HaCaT cells coculture on 3D-SFnws/ES hybrids and on Transwell

2.6.1. Preparation of the experimental group (HDFs and HaCaT cells cocultures on 3D-SFnws/ES hybrid scaffolds):

1) Three newly prepared and sterilized 3D-SFnws/ES hybrids were aseptically transferred with the rough 3D-SFnws side up into 6-well sterile, polystyrene culture plates with lid (SPL LIFE SCIENCES,

South Korea). Sterilized tweezers gently flattened the edges of the hybrids at the bottom of the plates.

2) Third or fourth passage HDFs were cultured under standard conditions (i.e. 37 ℃ in a 95% v/v air, 5% v/v CO_2 atmosphere) for 48 hours. It is worth noting that this time the culture medium was special, that is DMEM (89% v/v; Gibco, USA), bovine exosomes-depleted FBS (10% v/v; Gibico, USA), and penicillin-streptomycin solution (1% v/v; CAMBREX, Belgium). After detachment and collection, 1.0×10^5 HDFs were planted onto the rough 3D-SFnws surface of each hybrid sample.

3) Next, 5 mL of the same bovine exosome-depleted medium were added to each well. Then the cell culture was carried out under standard conditions (37 ℃ in a 95% v/v air, 5% v/v CO_2 atmosphere) for 48 hours.

4) Afterward, the spent culture medium was suctioned out of the wells. Next, the 3D-SFnws/ES hybrids samples were gently turned over thus having their smooth ES side up and their edges flattened with sterilized tweezers.

5) Third or fourth passage HaCaT cells were meanwhile cultured under standard conditions (i.e. 37℃ in a 95% v/v air, 5% v/v CO_2 atmosphere) for 48 hours using the same bovine exosome-depleted FBS medium. Once detached and collected,

1.0 × 10^5 HaCaT cells were seeded onto each smooth ES surface of the 3D-SFnws/ES hybrids.

6) Next 5 mL of the same bovine exosome-depleted medium was added to each well. Then the cell co-cultures were carried on under standard conditions (37 ℃ in a 95% v/v air, 5% v/v CO_2 atmosphere).

7) The same exosome-depleted fresh medium was added every 48 hours, while the cell-conditioned media samples were collected and stored at -80 °C.

2.6.2. The preparation of the control group (HDFs and HaCaT cells cocultures in Transwell systems):

1) Third or fourth passage HDFs and HaCaT cells were cultured under standard conditions (i.e. 37 ℃ in a 95% v/v air, 5% v/v CO_2 atmosphere) for 48 hours using the same bovine exosome-depleted medium.

2) After detachment, collection, and counting with a handheld automated cell counter (Scepter, Merck, Germany) 1.0 × 10^5 HDFs were planted onto the bottom of each of a total of 3 wells (the same 6-well sterile, polystyrene culture plates, SPL LIFE SCIENCES, South Korea).

3) After detachment, collection, and counting with a handheld automated cell counter (Scepter, Merck, Germany), 1.0 × 10^5

HaCaT cells were planted onto the bottom of each of three Transwell inserts (0.1μm pore size; 6 well format cell culture insert; FALCON, USA). Next, the inserts were at once put into the wells at whose bottoms the HDFs had been planted and 5mL of the same exosome-depleted FBS medium was added to each Transwell system. Then the cell cultures were carried out under standard conditions (i.e. 37 ℃ in a 95% v/v air, 5% v/v CO_2 atmosphere).

4) Changes of the same fresh bovine exosome-depleted medium were performed every 48 hours.

5) All of the coculture cell-conditioned media samples of both experimental and control groups were collected and spun at *2000* × *g* for 30 minutes at 4 ℃ to remove cells debris. The resulting supernatants were stored at −80℃ for later analysis.

2.7. Isolation and quantification of exosomes

After thawing each group of the supernatants, which had been collected according to the step 2.6, were pooled and the corresponding total exosome fractions were extracted using the Total Exosome Isolation Reagent for cell culture media (No. 4478359, Invitrogen, USA) following the manufacturer's protocol. The Isolation Reagent was added to supernatants (ration 1:1 v/v), and incubated overnight at 4 °C. Next, they were centrifuged again

for 90 minutes at *10,000* × *g* at 4 °C. The final pellets were the exosome fractions. This procedure has been compared with others and confirmed [41].

The total exosome proteins were quantified using Bradford's protein assay reagent (Bio-Rad, USA). Then, the marker-based assessments of exosomal preparations were conducted using two enzyme-linked immunosorbent assay (ELISA) kits that detect the CD9 marker (ExoTEST™, HansaBio Med, Estonia) and the CD81 marker (ExoELISA-ULTRA Complete Kit, SBI Systembio, USA). Notably, CD9 and CD81 are tetraspanin proteins intensely expressed by fibroblasts, and both typical markers present at the membrane surface of cell-released exosomes [42, 43]. Therefore, during subsequent experimental processing stages, identical quantities of exosomes proteins from the experimental and control groups were employed analyses in parallel.

2.8. Identification and quantitation of exosome-carried Inflammation factors (IFs) and AGFs

The several exosome-carried IFs and AGFs were respectively identified and quantified with the C-Series Human Angiogenesis Antibody Array C1000 (RayBiotech, USA) and C-Series Human Inflammation Antibody Array (RayBiotech, USA) according to the

manufacturer’s protocols.

Briefly, equal amounts of exosome proteins of the control and experimental group were diluted with PBS to 1.0ml for every sample. In the meantime, the antibody arrays membrane had been pre-treated for 30 minutes at room temperature with Odissey blocking buffer (LICOR, USA). Next, every membrane soaked with 1.0 ml sample and incubated overnight at 4 ℃. After repeated washings with two kinds of washing buffers, the array membranes were incubated for 2 hours with 1.0 ml of a mix of array-specific biotin-conjugated primary antibodies, diluted 1:250 in Odissey blocking buffer. Finally, Let every membrane was soaked in 2.0 ml DyLight800-conjugated streptavidin protein (Thermo Fisher, USA), diluted 1:7500 in Odissey blocking buffer, and incubated in the dark at room temperature for 1 hour. The positive signals of the several AGFs and IFs were acquired by using an Odissey scanner (LI-COR, USA) and their densitometric values quantified by using the Image Studio software package (version 5.2, LI-COR, USA). Each array’s positive signal intensity values were normalized via comparisons with correlated positive controls. The aggregated findings of three independent experiments were expressed as mean values ± standard deviations (SDs).

As comparing with traditional ELISA methods, this technology

has at least four advantages: (1) it allows for high-content screening using the same volume of samples; (2) it keeps ELISA-like sensitivity and increases the possibility of discovering key factors; (3) it has a wider detection range; and (4) it has a lower inter-array modulus of change between signal intensities of different array spots (5 - 10 %) [36].

2.9. Endothelial cells tube formation assay

1) The actual pro-angiogenic properties of the exosomes released from cells grown on 3D-SFnws/ES hybrids and Transwell system were assessed using in vitro cultured HDMVECs and the PromoKine Angiogenesis Assay Kit (No. PK-CA577-K905, PromoCell, Germany) according to the manufacturer's instructions.

2) HDMVECs were subcultured to 3rd passage under the standard conditions (i.e. 37 ℃ in a 95% v/v air, 5% v/v CO_2 atmosphere) in endothelial cell growth media, which include basal medium (95% v/v, No C-22210, PromoCell, Germany) and supplement mix (5% v/v, No C-39215, PromoCell, Germany).

3) Next, 3rd passage of HDMVECs were harvested using trypsin 0.025% v/v and counted with a handheld automated cell counter (Scepter, Merck, Germany).

4) The cell number was adjusted to 2.0 ×10^5/ml cell basal growth

medium fortified with 5% v/v exosome-depleted FBS.

5) Then, an aliquot (50 μL) of ECM solution was added to each well of a 96-well sterile cell culture plate kept on ice that was thereafter incubated at 37 ℃ to form a gel.

6) After that, 2.0×10^4 HDMVECs suspended in 100 μL culture medium were mixed with different concentrations (i.e. 0.5, 1.0, and 5.0 μg/ml) of exosomes from either the 3D-SFnws/ES hybrids group or the Transwell group, and directly added to each well. HDMVECs (2.0×10^4) without any exosomes added acted as the blank group (total 3 wells).

7) Finally, the plates were incubated at 37 ℃ in air with CO_2 5% v/v for 4 hours. The HDMVECs were checked at × 40 magnification under an inverted microscope (IM35, Zeiss, Germany) every hour.

8) Thereafter, the medium was removed and the wells were gently washed with 100 μL Wash Buffer. The Staining Dye working solution was added after removing the Wash Buffer. The cultures were then incubated for 30 minutes at 37 ℃ in the air with CO_2 5% v/v.

9) The wells were regularly observed under an inverted fluorescence microscope (IM35, Zeiss, Germany) fitted with proper excitation and emission filters and pictures were taken a C-P12 digital camera (OPTIKA, Italy) at 10× and 40× magnification.

10) The pictures were analyzed by means of Image J software. Triplicate results were averaged and expressed as the means ± SDs.

3. Statistical analysis

Statistical significance was determined using Student's "t" test for paired and unpaired samples: means differences with $P < 0.05$ were taken as significant.

Results

1. Morphological, physical, and chemical features of the 3D-SFnws/ES hybrids

The original 3D-SFnws are made by carded/hydroentangled SF fibers of a 10-14 μm diameter, 50 ± 7 mm length. They were 520 μm thick, weighed 58 g/m^2, and had a density of 105 g/m^3 [36].

The details of cross-section of this double sides scaffold were showed clearly in SEM images (Figure 1A). The scanning electron microscopy revealed the surface shape and micro structure of 3D-SFnws side very well (Figure 1B). For the novel 3D-SFnws/ES hybrids, the core feature was the electrospun layer made of SF nanofibers (average diameter in the 400-600 nm range) (Figure 1C). And the nanofibers/microfibers coupling was achieved at the interface by welding ones to the others during electrospinning. The details are shown at the fractured part in Figure 1D. Finally, the 3D-SFnws/ES hybrids were obtained by, attaching the thin upper layer of electrospun (ES) SF nanofibers to the surface of the 3D-SFnws. And the full thickness of the hybrid substrate was 0.82 ± 0.07 mm (determined according to UNI EN ISO 5084:1998).

The physical properties of this novel 3D-SFnws/ES hybrids

were characterized by attenuated total reflectance Fourier transform infrared spectroscopy (ATR-FTIR) and differential scanning calorimetry (DSC). The ATR-FTIR results showed the typical attenuated total reflectance of the new samples from the 2000 to 800 cm^{-1} wavenumber range. This spectral spectrum is the fingerprint of SF, as it exhibits multiple absorption bands that are heavily influenced by its physical and chemical structure [44, 45]. These 3D-SFnws/ES hybrids had two sides with completely different characteristics, even though they were made of the same fiber. As a result, each side had its own set of data (Figure 1E) . On the 3D-SFnws side, the bands (a) of Amide I at 1623 cm^{-1}, with shoulder at 1695 cm^{-1}, Amide II at 1514 cm^{-1} and Amide III at 1228 cm^{-1}, with a shoulder at about 1258 cm^{-1}, were typical of the β-sheet molecular conformation of crystalline and oriented SF fibres. The ES sideband (b) at 1725 cm^{-1} is typical of electrospun SF nanofibers, being attributed to residual formic acid bound to SF as formate. Figure 1F shows the thermogram of the 3D-SFnws/ES hybrids obtained by using differential scanning calorimetry (DSC). It has a prominent melting/degradation peak at 317 °C, and a shoulder at about 290 °C (arrow) representing the contribution of the ES layer to the degradation of the hybrids, which is typical of SF fibres with a high degree of molecular order and crystallinity [45].

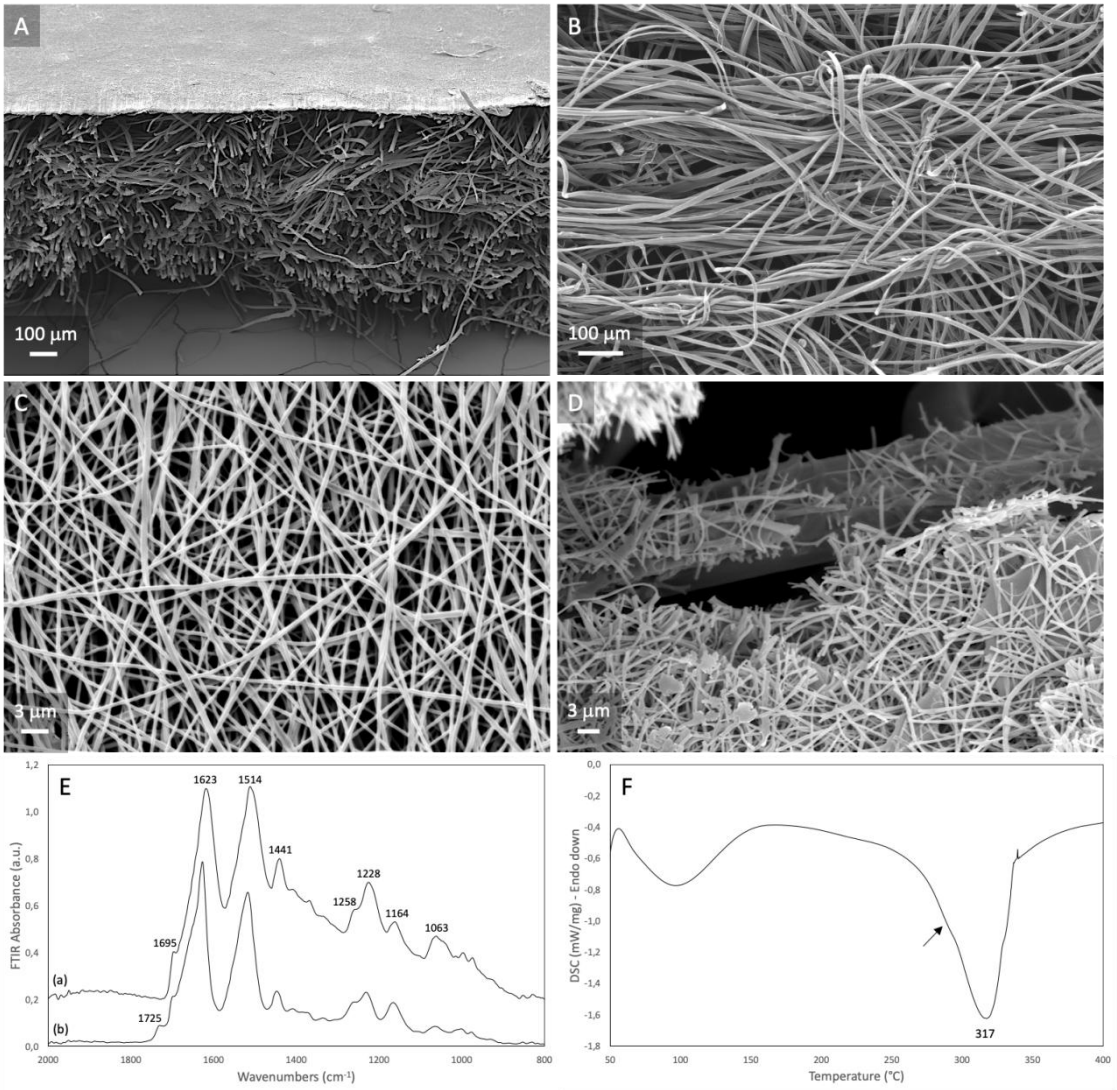

Figure 1. A-D: SEM images of the 3D-SFnws/ES hybrids substrate. **A**. Cross-section showing the thin upper layer of electrospun (ES) SF nanofibers attached to the surface of the 3D-SFnw. **B**. Detail of the 3D-SFnws made of SF microfibers. **C**. Detail of the electrospun layer made of SF nanofibers. **D**. Detail of a fractured area showing that nanofibers/microfibers coupling is achieved at the interface by welding ones to the others during electrospinning. **E**. Attenuated total reflectance Fourier transform infrared spectroscopy (FTIR) spectra in the 2000 cm^{-1} to 800 cm^{-1} wavenumber range of the 3D-SFnws/ES hybrids: (a) 3D-SFnw side; (b) ES side. **F**. Differential scanning calorimetry (DSC) thermogram of the 3D-SFnws/ES hybrids.

2. Growth and metabolism of HDFs and HaCaT cells grown on 3D-SFnws/ES hybrids

2.1. Growth and metabolism of HDFs grown on 3D-SFnws/ES hybrids

After careful planting, about 85% of the intravitally labelled HDFs adhered to the 3D-SFnws/ES hybrids within 4 hours. Microscopy investigations corroborated the numerical rise of HDFs over time (Figure 2a, b, c, d). The development of adherent cells was paralleled by a 4.7-fold rise in the quantity of double-strand DNA associated with 3D-SFnws/ES hybrids between experimental days 3 and 15. (Figure 2e). Biochemical studies revealed that the cumulative D-Glucose consumption of HDFs adhering to 3D-SFnws side rose 5.3-fold between experimental days 3 and 15, i.e. paralleling the HDFs numerical increases (Figure 2f). The results of this part are close to our previous studies of 3D-SFnws [36]. The number of cells attached to fibers is higher than in the previous experiments. The most likely reason is that the new 3D-SFnws/ES hybrids were combined with the thin layer of ES SF, so during the seeding procedure the cells did not pass through the holes of the original 3D-SFnws thereby partially adhering to the polystyrene surface underneath.

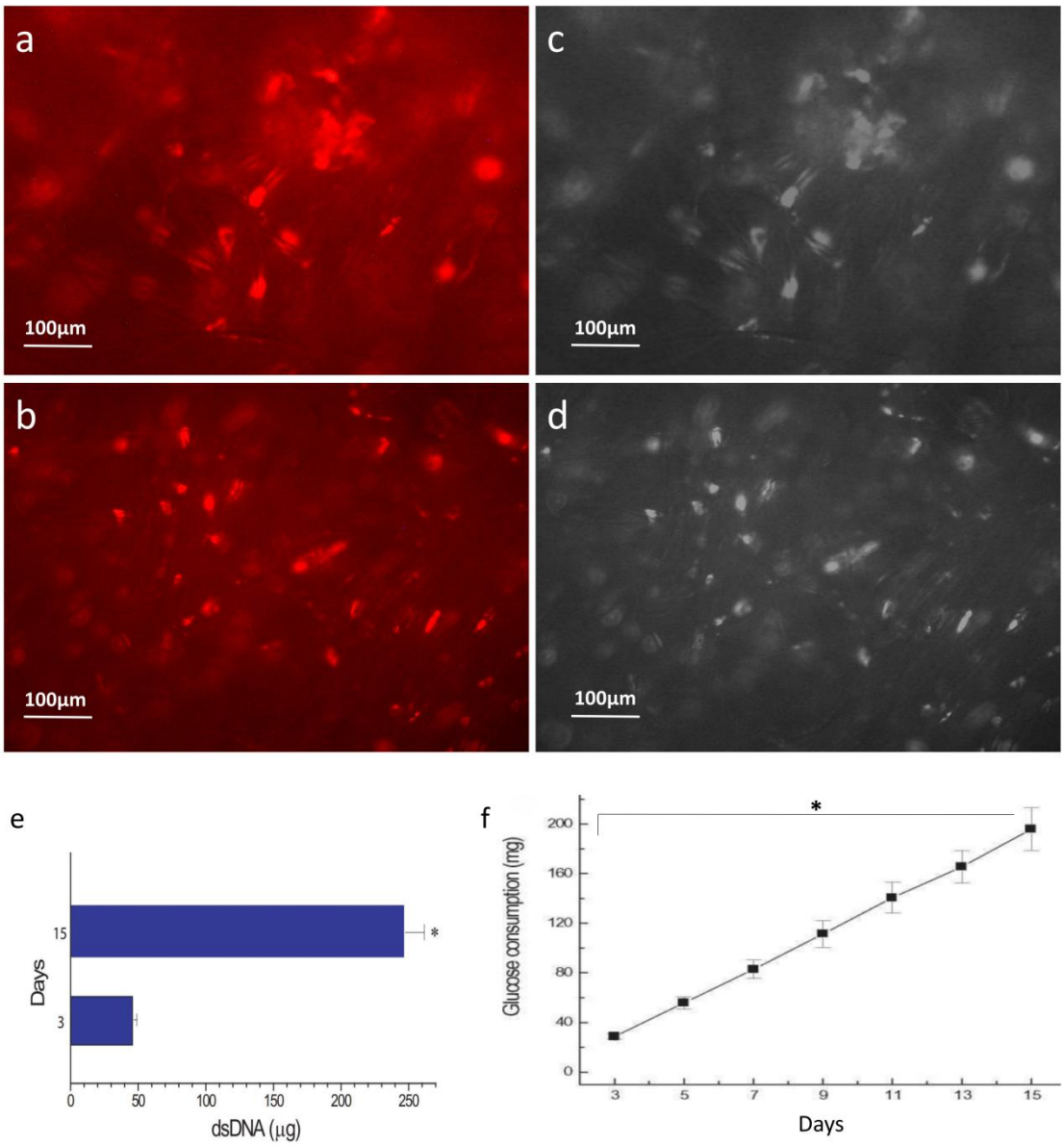

Figure 2. HDFs adhered to and colonized the 3D-SFnws side of 3D-SFnws/ES hybrids, and their morphology, growth, and metabolic activity were studied. (**a, b**) Due to the lipophilic stain incorporated by their cellular membranes, HDFs on 3D-SFnws/ES hybrids emit a red fluorescence at λ 565 nm when viewed via a fluorescence inverted microscope.The microfibers emit no interfering fluorescence at λ 565 nm and are hence barely noticeable. Because the visible cells are linked to a 3D scaffold, the majority of them are obviously out of focus. However, at 5 days (**b**), cell numbers are considerably larger than at 2 days after plating (**a**). (**c, d**) These are the same images as in (**a**) and (**b**), but after the red colour has been removed digitally by the image software.Under these conditions, it is feasible to discern very thin black stripes at some places running in parallel, which correspond to the SF microfibers. Some of these stripes run over and cut the underlying cells. (**e**) HDFs attached to fibers significantly increase in quantity over the course of 15 days in vitro, as seen by a 4.7-fold increase in the number of cells adhering to the scaffolds between day 3 and day 15. The quantities of double strand (ds) DNA were determined as described in the Methods. The bars represent the mean value ± standard

deviation (SD) of three different duplicate determinations at each time point, *p < 0.01. (**f**) The total D-Glucose intake of HDFs grown on 3D-SFnws/ES hybrids. D-glucose levels in conditioned medium were measured at each time point as described in the Methods. Each dot indicates the mean value ± standard deviation from three different duplicate determinations, *p < 0.01.

2.2. Growth and metabolism of HaCaT cells grown on 3D-SFnws/ES hybrids

After 4 hours of meticulous planting, 80-90% of the intravitally dyed HaCaT cells attached to the 3D-SFnws/ES hybrids. Microscopy studies confirmed the numerical increase of HaCaT cells over time (Figure 3a, b, c, d). The growth of the adherent cells was accompanied by a 6.5-fold increase in the amount of double-strand DNA associated with 3D-SFnws/ES hybrids between experimental days 3 and 15 (Figure 3e). Biochemical analyses proved that the cumulative D-Glucose consumption of HaCaT cells adhering to the ES side of 3D-SFnws/ES hybrids increased 6.2-fold in culture between experimental days 3 and 15, which corresponded to HaCaT cells numerical increases (Figure 3f).

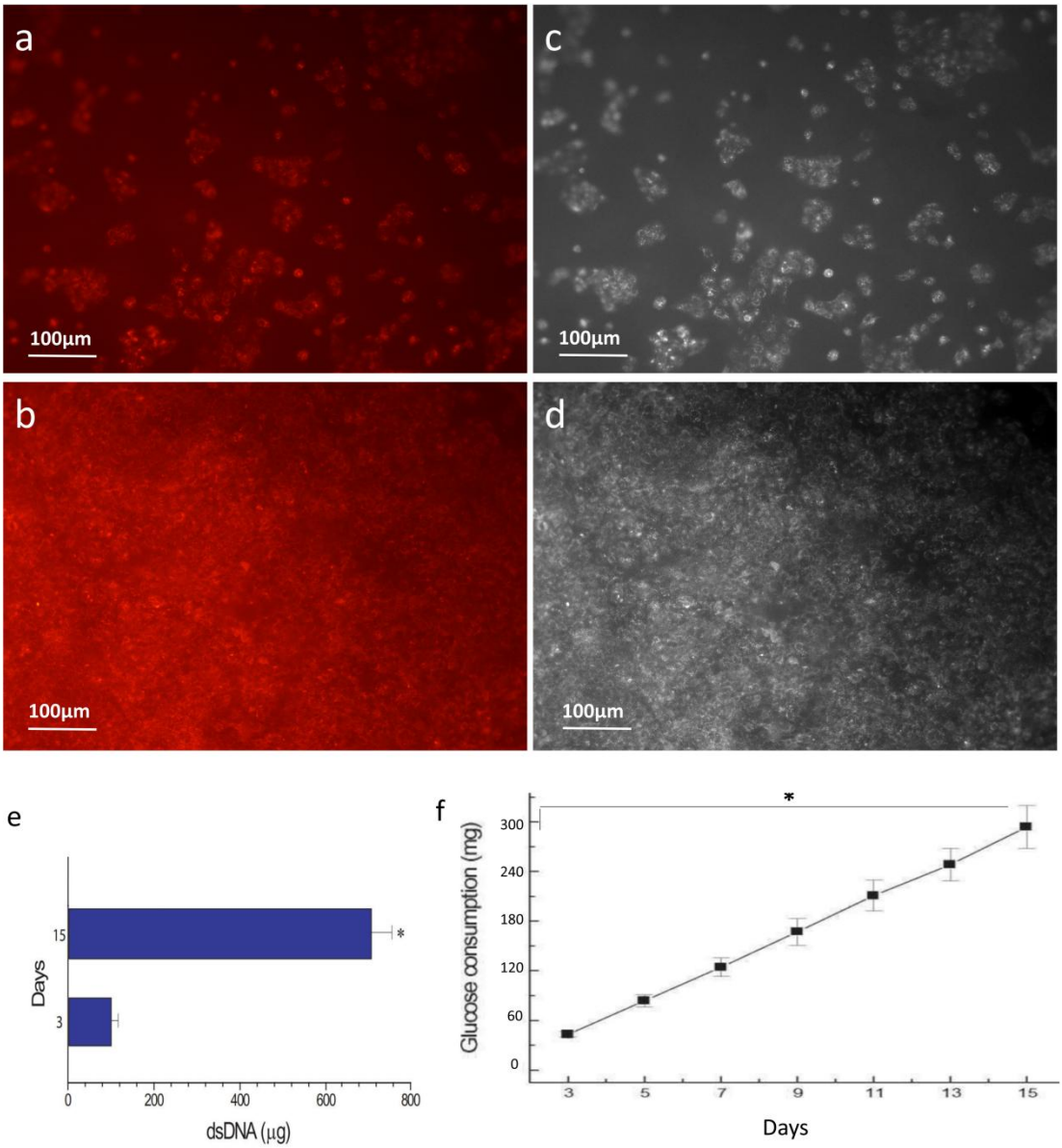

Figure 3. HaCaT cells attached to and colonized the ES side of 3D-SFnws/ES hybrids, and their morphology, growth, and metabolic activity were studied. (**a, b**) Due to the lipophilic stain incorporated by their cellular membranes, HaCaT cells on 3D-SFnws/ES hybrids emit a red fluorescence at λ 565 nm when viewed via a fluorescence inverted microscope. The ES layer does not emit interfering fluorescence at λ 565 nm and the nanofibers of ES layer are much denser than 3D-SFnws. Thus, HaCaT cells adhered to the ES side of 3D-SFnws/ES hybrids are similar to growing on polystyrene. However, at 7 days (**b**), cell numbers are fairly larger than at 2 days after plating (**a**). (**c, d**) These are the same images as in (**a**) and (**b**), but after the red color has been removed digitally by the image software. At this magnification, the background, which is the surface of dense ES SF nanofibers, appears very clean. (**e**) HaCaT cells attached to surface of ES layer significantly increase in quantity over the course of 15 days in vitro, as seen by a 6.5-fold increase in the number of cells adhering to the scaffolds between day 3 and day 15. The quantities of double strand (ds) DNA were determined as described in the Methods. The bars represent the mean value ± standard deviation (SD) of three different duplicate

determinations at each time point, *p < 0.01. (**f**) The total D-Glucose intake of HaCaT cells grown on 3D-SFnws/ES hybrids. D-glucose levels in conditioned medium were measured at each time point as described in the Methods. Each dot indicates the mean value ± standard deviation from three different duplicate determinations, *p < 0.01.

3. Inflammation Factors (IFs) amounts released via exosomes from HDFs and HaCaT cells cocultured on 3D-SFnws/ES hybrids and in Transwell systems

The specific double-antibody membrane arrays allowed us to identify and quantify the IFs carried by same amounts of exosomes proteins from HDFs and HaCaT cells cocultured on 3D-SFnws/ES hybrids and in Transwell system [46].

Figures 4a and 4b show typical developed array membranes (one membrane for each group) covering the whole range of agents tested. The array results revealed that 14 of the 40 potentially discoverable IFs were carried by the exosomes released from HDFs and HaCaT cells of both experimental groups (Figures 4 and 5; Table 2). The quantitative measurement and statistical comparison of matching spots revealed that the levels of 7 types of exosome-carried IFs (14 in total) from the 3D-SFnws/ES group were considerably higher than their counterparts of the Transwell group (Figure 5; Table 2). The highest percent increases in the 3D-SFnws/ES group vs. the Transwell group were those of

Interleukin-8 (IL-8; +271.6%), Monocyte chemoattractant protein-1 (MCP-1; +187.6%), and Macrophage Inflammatory Protein-1α (MIP-1α; +54.3%). Lesser (< 50%) but still significant increases in the 3D-SFnws/ES group vs. the Transwell group pertained to eosinophil chemotactic protein 2 (Eotaxin-2 or Chemokine [C-C motif] ligand 24, CCL2; +45.6%), Interleukin-10 (IL-10; +45.3%), Macrophage colony-stimulating factor (M-CSF or Colony stimulating factor 1, CSF1; +38%), and Tissue inhibitor of metalloproteinase-2 (TIMP-2; +43.1%). Conversely, the amounts of the remaining 7 compounds conveyed by the exosomes did not show any significant ($p > 0.05$) difference between the two groups. The latter included Interleukin-3 (IL-3), Interleukin-16 (IL-16), Interferon γ-induced protein 10 (IP-10 or C-X-C motif chemokine ligand 10, CXCL10), Macrophage Inflammatory Protein-1β (MIP-1β), RANTES (Chemokine [C-C motif] ligand 5, CCL5), and Tumor necrosis factor α, β (TNF-α, -β). (Table 2).

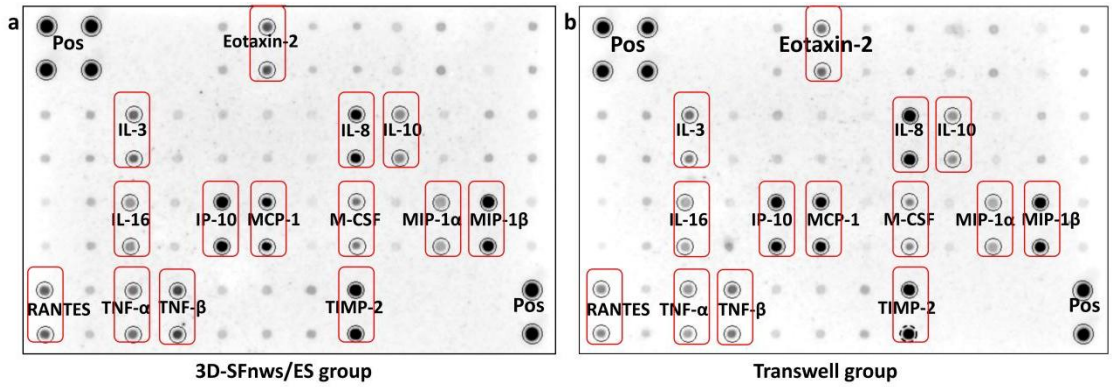

Figure 4. Developeddouble-antibody array membranes (each array made of 1 membrane) showing the IFs carried by the exosomes released from HDFs and HaCaT cells grown either on 3D-SFnws/ES hybrids (**a**), or on Transwell system as control group (**b**). Equal amounts of exosomes isolated from conditioned media samples of the 2 groups were used. The red rectangles include the duplicate dots of 14 expressed exosome-carried IFs.

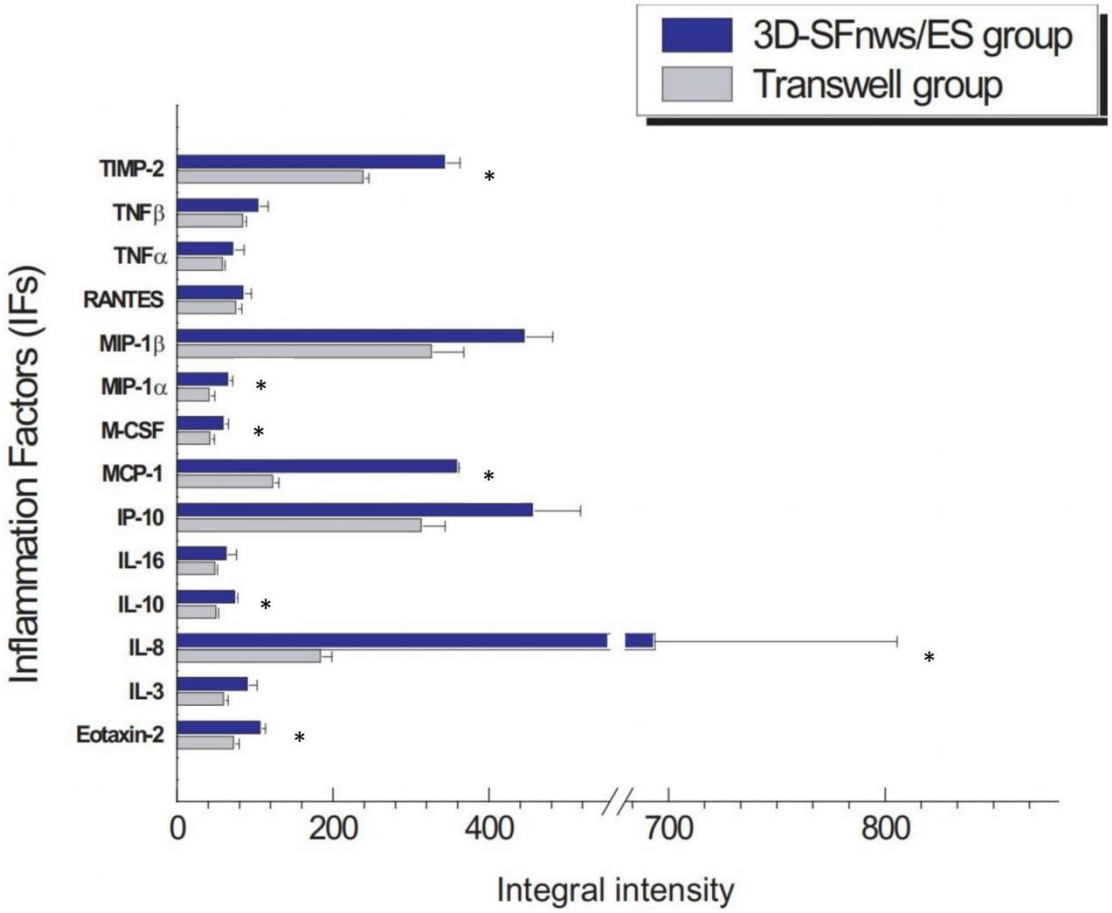

Figure 5. The integral intensities of 14 IFs between the 3D-SFnws/ES hybrids group and Transwell system group are shown by the length of bars. And the amounts of the 7 compounds of exosomes show the significant (* $p < 0.05$) difference between the two groups, including Eotaxin-2, IL-8, IL-10, MCP-1, M-CSF, MIP-1α, and TIMP-2.

Table 2. IFs carried by equal amounts of exosomal proteins from either group

IFs	Transwell group	3D-SFnws/ES group	Δ %	*P* value
Eotaxin-2	75. 08 ± 4.57	109. 32 ± 4.17	+45.6	< 0.05
IL-3	62.75 ± 2.84	92.93 ± 9.98	+48.1	0.054
IL-8	186.63 ± 12.05	693.60 ± 111.97	+271.6	< 0.05
IL-10	52.85 ± 0.61	76.79 ± 1.26	+45.3	< 0.01
IL-16	51.51 ± 0.29	65.95 ± 10.38	+28.0	0.188
IP 10	315.74 ± 27.95	458.66 ± 58.60	+45.3	0.09
MCP-1	125.58 ± 5.05	361.20 ± 0.13	+187.6	< 0.01
M-CSF	44.98 ± 2.79	62.06 ± 3.73	+38.0	< 0.05
MIP-1α	44.17 ± 4.19	68.17 ± 3.25	+54.3	< 0.05
MIP-1β	328.86 ± 38.78	447.82 ± 33.93	+36.2	0.082
RANTES	78.07 ± 5.12	87.49 ± 7.96	+12.1	0.295
TNFα	61.15 ± 0.64	74.09 ± 12.00	+21.2	0.268
TNFβ	87.05 ± 1.90	106.37 ± 10.50	+22.2	0.125
TIMP-2	241.69 ± 4.37	345.95 ± 16.78	43.1	< 0.05

The data represent the mean values ± standard deviations of densitometric integral intensity evaluations for each component from three separate experiments with triplicate determinations. The numbers displayed are the original values × 10^3.

4. Angiogenic growth factors (AGFs) amounts released via exosomes from HDFs and HaCaT cells cocultured on 3D-SFnws/ES hybrids and in Transwell system

Specific array membranes (2 membranes for each group) allowed us to test a series of AGFs. The array results revealed that 14 of the 43 potentially discoverable AGFs were conveyed by

exosomes released from HDFs and HaCaT cells belonging to either experimental group (Figures 6 and 7; Table 3). The quantitative measurement and statistical comparison of matching spots revealed that the levels of 12 of the 14 exosome-carried AGFs from the 3D-SFnws/ES group were considerably higher and instead 2 others lower than their counterparts in the exosomes of the Transwell group (Figure 7; Table 3). The highest percent increases in the 3D-SFnws/ES group vs. the Transwell group were those of Monocyte chemoattractant protein-1 (MCP-1; +789.6%), and Growth-regulated oncogene (GRO; +357.2%). The lesser but still significant (> 50%) increases in the 3D-SFnws/ES group versus the Transwell group were those of Tissue inhibitor of metalloproteinase-1 (TIMP-1; +54.5%), TIMP-2 (+56.8%), Matrix metallopeptidase 9 (MMP-9; +69.6%). On the other hand, the amounts of the remaining 9 compounds of exosomes did not show the significant ($P > 0.05$) difference between the two groups. The latter included basic fibroblast growth factor (bFGF), vascular endothelial growth factor D (VEGF-D), Angiopoietin 1 (ANGPT1), ANGPT2, Angiotensin, Angiopoietin-1 receptor (Tie-2), urokinase plasminogen activator surface receptor (uPAR), and vascular endothelial growth factor receptor 3 (VEGFR3) (Table 3).

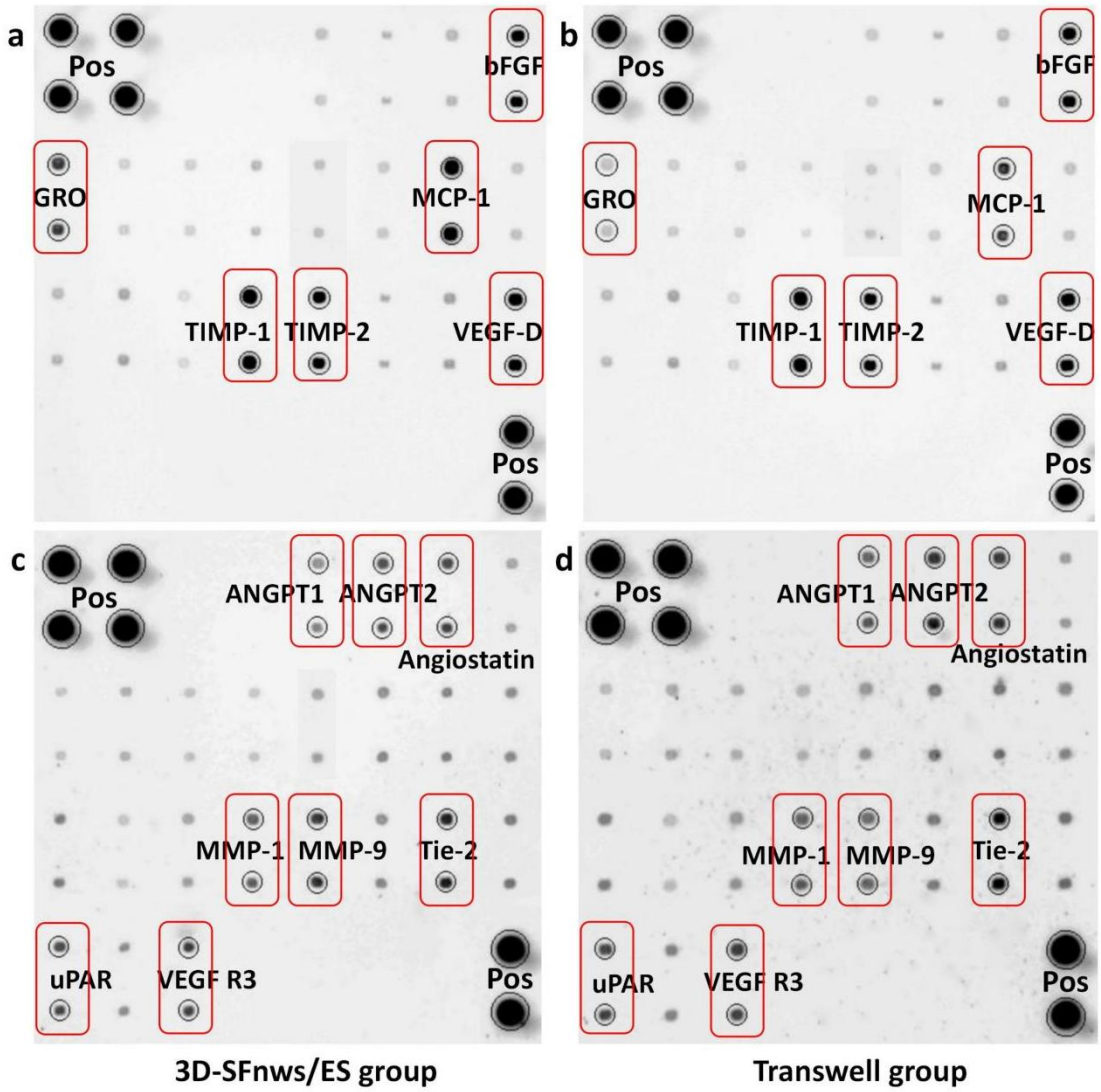

Figure 6. The double-antibody array membranes (each array made of 2 different membranes) showing the AGFs carried by the exosomes released from HDFs and HaCaT cells grown either on 3D-SFnws/ES hybrids (**a, c**), or on Transwell system as the control group (**b, d**). Equal amounts proteins from the exosomes isolated from conditioned media samples of the 2 groups were used. The red rectangles include the duplicate dots of total 14 exosome-carried IFs.

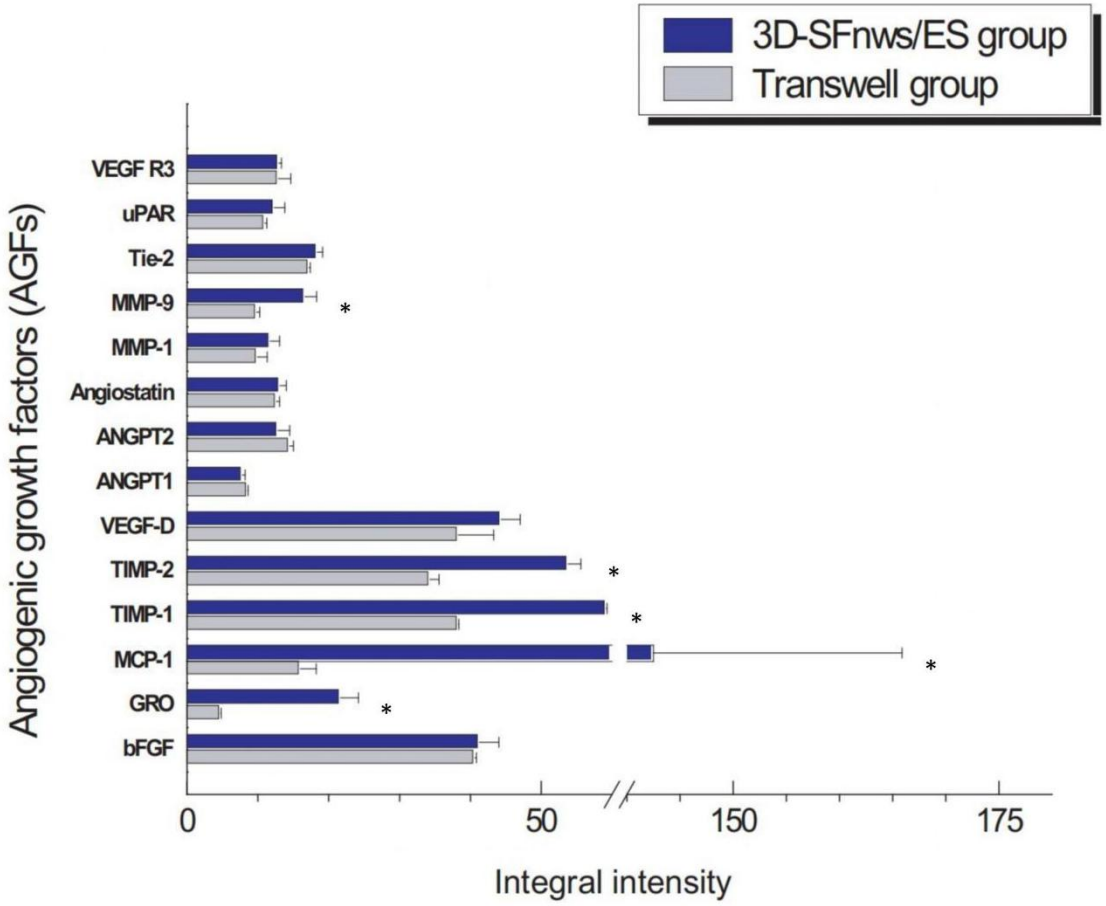

Figue 7. The different integral intensities of 14 AGFs between the 3D-SFnws/ES hybrids group and Transwell system group are shown. And the amounts of 5 AGFs show a significant (* $p < 0.05$) difference between the two groups, including GRO, MCP-1, TIMP-1, TIMP-2, MMP-9.

Table 3. AGFs carried by equal amounts of exosomal proteins from either group

AGFs	Transwell group	3D-SFnws/ES group	Δ %	*P* value
bFGF	40. 65 ± 0.22	41. 28 ± 2.74	+1.6	0.777
GRO	4.74 ± 0.08	21.66 ± 2.57	+357.2	< 0.05
MCP-1	16.01 ± 2.24	142.45 ± 23.43	+789.6	< 0.05
TIMP-1	38.33 ± 0.04	59.22 ± 0.07	+54.5	< 0.01
TIMP-2	34.31 ± 1.28	53.80 ± 1.80	+56.8	< 0.01
VEGF-D	38.33 ± 4.99	44.34 ± 2.71	+15.7	0.237
ANGPT-1	8.58 ± 0.04	7.84 ± 0.34	-8.7	0.092
ANGPT-2	14.48 ± 0.54	12.86 ± 1.62	-11.2	0.312
Angiostatin	12.65 ± 0.43	13.11 ± 0.87	+3.7	0.564
MMP-1	9.92 ± 1.39	11.75 ± 1.32	+18.5	0.082
MMP-9	9.82 ± 0.44	16.15 ± 1.63	+69.6	< 0.05
Tie-2	17.22 ± 0.15	18.42 ± 0.72	+7.0	0.147
uPAR	10.99 ± 0.26	12.30 ± 1.50	+12.0	0.348
VEGF R3	12.88 ± 1.75	12.94 ± 0.23	+0.4	0.966

The data represent the mean values ± standard deviations of densitometric integral intensity evaluations for each component from three separate experiments with triplicate determinations. The numbers displayed are the original values × 10^3.

5. Induction of human endothelial cells tube formation by exosome released from HDFs and HaCaT cells cocultured on 3D-SFnws/ES hybrids and in Transwell systems

In our earlier work, we investigated whether AGFs carried by exosomes released from 3D-SFnws-adhering HDFs might have triggered HDMVECs to form tubes *in vitro*. The result was

affirmative [36]. In this study, we assessed whether the exosome released from two types of cells cocultured in two different environments, i.e. 3D-SFnws/ES hybrids and Transwell system, could induce HDMVECs to form tubes in vitro. The results showed that such exosomes had angiogenic potency (Figure 8). Once seeded for 2 hours onto the ECM gel, the HDMVECs treated with the exosome-added medium started making connections. Then after 4 hours, the majority of the HDMVECs treated with the medium added with the exosomes released from HDFs and HaCaT cells cocultured on 3D-SFnws/ES hybrids formed endothelial tubes filling all the microscopic fields (Figure 8b2, c2, d2). However, HDMVECs cultured with the control medium (i.e. basal medium with 5% v/v exosome-depleted FBS but no exogenous exosomes added) showed very limited amounts of initial endothelial tubes (Figure 8a1, a2). On the other hand, the exosomes released from HDFs and HaCaT cells cocultured in the Transwell system also strongly induced HDMVECs to form endothelial tubes in vitro even at the lower concentrations (Figure 8b1, c1, d1). The number of the endothelial cell tubes per microscopic field (40× magnification) did not significantly differ ($P > 0.05$) between two groups with the same exosome concentration or even between different exosome concentrations in the same group (Figure 8e).

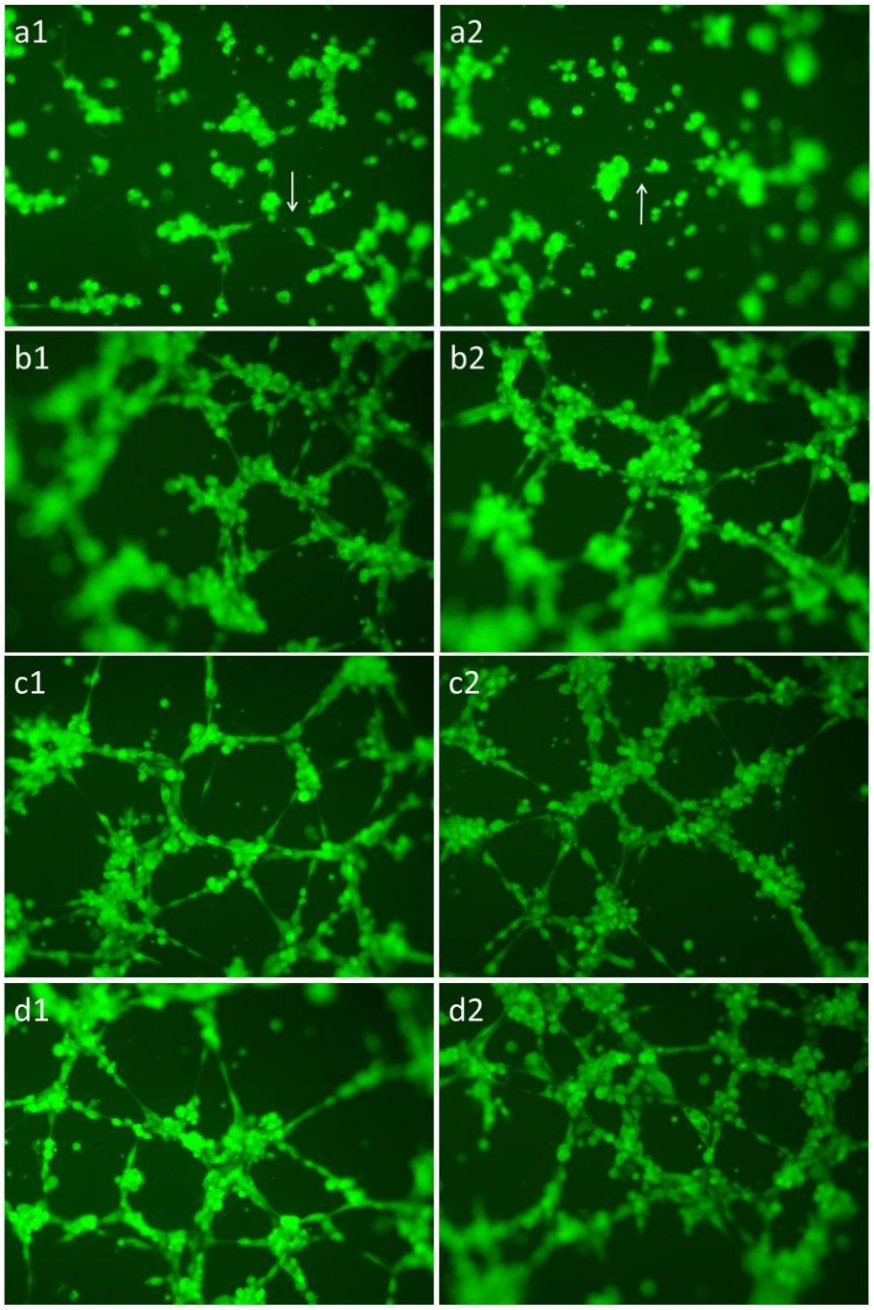
a1
a2
b1
b2
c1
c2
d1
d2

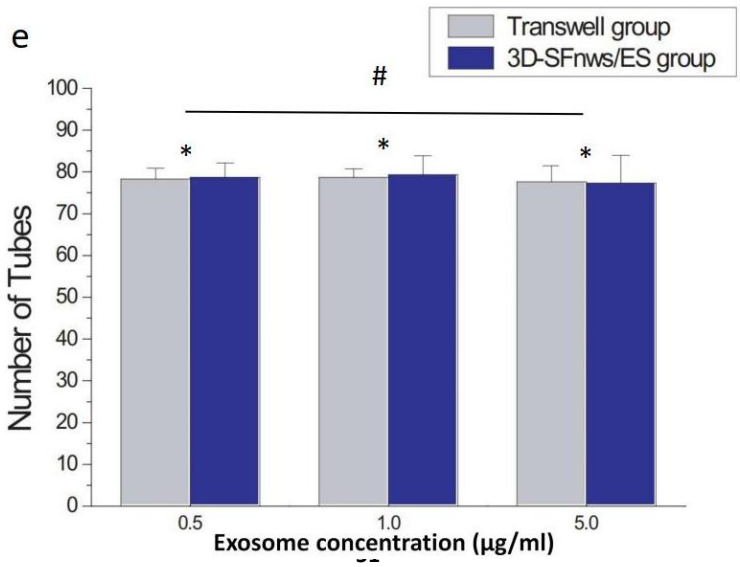
e
Transwell group
3D-SFnws/ES group
#
*
*
*
Number of Tubes
0
10
20
30
40
50
60
70
80
90
100
0.5
1.0
5.0
Exosome concentration (μg/ml)

Figure 8. Exosomes released from HDF and HaCaT cells coculture in 3D-SFnws/ES hybrids and in Transwell system induce human dermal microvascular endothelial cells (HDMVECs) to form tubes *in vitro*. (**a1, a2, b1, b2, c1, c2, d1, d2**) After seeding onto extracellular matrix (ECM) gel 4 hours and staining with dye working solution, micrograph showing HDMVECs emit a green fluorescence at λ 510 nm when viewed via a fluorescence inverted microscope. (**a1, a2**) The blank group ,which are HDMVECs cultured on basal medium fortified with 5% v/v exosome-depleted FBS, showing that HDMVECs just start to connect the nearby cells at this moment (arrows). (**b1, b2, c1, c2, d1, d2**) However, at this moment numbers of tubes have been formed. (**b1, c1, d1**) HDMVECs were cultured on conditional medium (basal medium fortified with 5% v/v exosome-depleted FBS) mixed exosomes released from HDF and HaCaT cells coculture in Transwell system with concentrations 0.5, 1.0, and 5.0 μg/ml. (**b2, c2, d2**) HDMVECs were grown in conditional media (basal medium fortified with 5% v/v exosome-depleted FBS) with 0.5, 1.0, and 5.0 g/ml concentrations of mixed exosomes produced from HDF and HaCaT cells coculture in 3D-SFnws/ES hybrids. (**f**) The total number of tubes was counted by Image J on pictures taken at ×40 magnification for all of 3 wells for each exosome concentration. Triplicate results were averaged and the bars show the mean values ± standard deviations (SD). There is no statistical difference ($P > 0.05$) between groups (*) at the same exosome concentration or between different exosome concentrations in the same group (#).

Discussion

1. 3D-SFnws/ES hybrids

As is well known, human skin is composed of four main regions: the stratum corneum, the viable epidermis, dermis, and subcutaneous tissues, and a number of appendages are associated with the skin: hair follicles, and eccrine and apocrine sweat glands [47]. There is no doubt that the dermis is the scaffold and main component of the entire skin. It is about 2-5 mm in thickness and consists of collagen fibrils that supply support and elastic connective tissue that provides elasticity and flexibility, embedded within a mucopolysaccharide matrix. Within this matrix is a sparse cell population, including fibroblasts that produce the components of the connective tissue (collagen, laminin, fibronectin, vitronectin), mast cells involved in the immune and inflammatory response, and melanocytes responsible for pigment production. Within the dermis is present an extensive vascular network that acts to regulate body temperature, provides oxygen and nutrients to, and removes toxins and waste products from tissues, and facilitates immune response and wound repair.

Therefore, SF, as a potential natural biological material, must

have two basic conditions to be conformed into a tissue engineering dermal scaffold besides being suited to fulfill the mechanical requirements of soft tissues: First, dermal cells, mainly fibroblasts, should attach and proliferate on the scaffold to produce ECM. Second, an extensive vascular network should form within the scaffold. In our earlier study, we had produced thicker and mechanically more robust scaffolds by increasing the length of the SF microfibers. Then, we also proved that this novel 3D SF nonwovens (3D-SFnws) displayed excellent handling stability (could be cut to any needed size and form) and allowed to modulate the biomechanical responses across a wider range of stress and strain values. We confirmed that HDFs can grow and proliferate well on the 3D-SFnws and that the exosomes released from 3D-SFnws-adhering HDFs exerted a powerful proangiogenic stimulus on HDMVECs *in vitro* [36].

However, the requirement of an ideal artificial dermal scaffold that cannot be ignored is that it should support also the growth and metabolism of the epidermal cells required to reform an epidermis. In human skin, the epidermis is a multilayered region that varies in thickness from about 0.06 mm on the eyelids to about 0.8 mm on the palms of the hands and soles of the feet. Because the epidermis lacks its own blood vessels, the epidermal cells must

obtain nutrients and discharge waste through a bidirectional diffusion process across the epidermal-dermal basal lamina and the cutaneous circulation. The epidermis is in a constant state of renewal, with the formation of a new cell layer of keratinocytes at the basal layer, and the loss of their nucleus and other organelles to form desiccated, proteinaceous corneocytes on their journey toward desquamation [48], which in normal skin occurs from the skin surface at the same rate as that of keratinocytes neoformation [49]. Thus, for the epidermal cells to grow flat on the SF scaffold, the structure of 3D-SFnws had to be improved.

To retain all the advantages of the original 3D-SFnws, we redesigned a new hybrid scaffold by adding a flat layer of relatively dense SF nanofibers. Electrospinning (ES) was considered the best choice to produce the layer of SF nanofibers. Finally, the 3D-SFnws/ES hybrid was produced, which has a layer of ES SF nanofibers deposited on one of its sides. Therefore, this novel 3D-SFnws/ES hybrid has two different sides, the rough 3D-SFnws side and the smooth ES side.

Not only the proper tests have verified that 3D-SFnws/ES hybrids basically keep the original physical, and chemical features of the old 3D-SFnws (Figure 1), but also the experimental results have shown that HDFs adhered to and colonized the 3D-SFnws

rough side (Figure 2). What is even more exciting is that the keratinocytes, the typical epidermal cell, also can attach and grow well on the smooth ES side of 3D-SFnws/ES hybrids (Figure 3).

2. AGFs released via exosomes from HDFs and HaCaT cells cocultured on 3D-SFnws/ES hybrids induce human endothelial cells to form tubes *in vitro*

In our previous work, we used for comparison purposes the HDFs grown on polystyrene. Our results proved that the exosomes released from 3D-SFnws-adhering HDFs carried significant surpluses of 10 AGFs, and that the same amounts of exosomes powerfully stimulated HDMVECs to produce significant amounts of endothelial tubes *in vitro* [36]. Conceivably, this locally generated neoangiogenesis will improve the chances of success for SF nonwoven as implants promoting wound healing. However, in the present study, the cells' microenvironment has changed, not only because of the added structural nanofibers, but also because of the addition of another cell type.

Similarly, we also demonstrated the statistically significant expression of 5 AGFs in the exosomes released from cocultured HDFs and HaCaT cells on the 3D-SFnws/ES hybrids (Figures 6

and 7). The number of enriched factors is less in the exosomes released from two different cell types than in the previous study that only tested a single cell type [36]. Among the former AGFs, the expression of the growth-regulated oncogene (GRO) was higher in the 3D-SFnws/ES hybrids group than in the Transwell group (control group). The GRO, or chemokine (C-X-C motif) ligand (CXCL) family is also collectively called neutrophil-activating protein 3 (NAP-3). This family includes GRO-α/CXCL1, GRO-β/CXCL2, and GRO-γ /CXCL3, which are the products of three distinct, non-allelic genes. The GRO/CXCL members act as chemoattractants for several kinds of immune cells, especially neutrophils or other non-hematopoietic cells, guiding them to the sites of injury or infection, thus playing an important role in the regulation of immune and inflammatory responses [50, 51]. GRO-α/CXCL1 attracts neutrophils, is upregulated in acute wounds and, by promoting keratinocyte migration, advances wound reepithelization [52, 53]. GRO-β/CXCL2 chemokine plays an important role in the normal breaking of the junctions between endothelial cells [54]. In addition, the expression of monocyte chemoattractant protein 1(MCP-1) was also significantly higher in the exosomes from the hybrid SF scaffold than from the Transwell system. MCP-1, also referred to as the chemokine (C-C motif)

ligand 2 (CCL2), is a small cytokine that belongs to the CC chemokine family. MCP-1 attracts monocytes, memory T cells, and dendritic cells to inflammatory areas caused by tissue damage or infection [55, 56]. A recent study using diabetic mice showed that MCP-1 can reverse an impaired skin wound healing by normalizing the neovascularization and collagen accumulation [57]. Chemokines (e.g. MCP-1, CCL21, etc.) are key regulators of the wound healing process, and they are involved in the promotion and inhibition of angiogenesis and the recruitment of inflammatory cells, the latter also releasing growth factors and cytokines to ease the wound healing process [58]. The observed induction of human endothelial cells tube formation by exosomes released from HDFs and HaCaT cells co-grown on 3D-SFnws/ES hybrids (Figure 8), is consistent with the presence of significantly enriched amounts of cytokines and chemokines like GRO and MCP-1, which mainly advance angiogenesis. On the other hand, MMP-9 (matrix metallopeptidase 9) is a classical zinc-metalloproteinase enzyme that is involved in the breakdown of the ECM. Using a MMP9-deficient mouse model, it was seen that MMP-9 coordinated epithelial wound repair as the MMP9-deficient mice were unable to remove the fibrinogen matrix during wound healing [59]. When interacting with transforming growth factor-β (TGF-β), MMP-9 also

stimulates collagen fiber retraction, thus aiding wound closure [60]. Both Tissue inhibitors of metalloproteinase-1 (TIMP-1) and TIMP-2 are members of the TIMP family. Matrix metalloproteinases (MMPs), a group of peptidases involved in the breakdown of the extracellular matrix, are naturally inhibited by these glycoproteins. As a result, these encoded proteins may be critical to the maintenance of tissue homeostasis by remodeling of the ECM [61]. TIMP-1 can strongly inhibit MMP-9 and MMP-1 [62]. Thus, the expression of these three protein factors has a certain degree of correlation. It is valuable to mention here that an increased expression of both TIMP-1 and TIMP-2 can stabilize the basement membrane and regulate ECM remodeling at the level of wound beds [63]. In summary, the improved 3D-SFnws/ES hybrids based on 3D-SFnws still retain some of the original excellent features, which are the promotion of angiogenesis and the positive regulation of ECM remodeling.

3. IFs released via exosomes from HDFs and HaCaT cells cocultured on 3D-SFnws/ES hybrids

Clearly, the granulation tissue forms during the wound-healing process, which begins with an inflammation-dominated phase. Fibroblasts (mesenchymal cells) are maximally stimulated in the

granulation tissue, and multiply producing massive amounts of ECM. Conversely, the epithelial cells (keratinocytes) proliferate and migrate on the underlying granulation tissue's temporary matrix, finally sealing the wound defect. So many pieces of evidence suggest that keratinocytes drive fibroblasts to produce growth factors, which then stimulate keratinocyte proliferation in a bidirectional paracrine fashion in the above dynamic process [26, 64]. This phenomenon is named "Keratinocyte-Fibroblast Interactions". At the early stages of wound healing, proinflammatory mediators such as keratinocyte-derived IL-1 dominate the keratinocyte-fibroblast interactions [65, 66]. At this time, the TGF-β activity is also strongly up-regulated in the keratinocyte-fibroblast interactions, but the activation of nuclear factor kappa-light-chain-enhancer of activated B cells (NF-κB) occurs when the TGF-β signaling pathway is blocked in the fibroblasts. Then, factors such as IL-6, Keratinocyte growth factor (KGF), Granulocyte-macrophage colony-stimulating factor (GM-CSF), and endothelin-1 (ET-1), are up-regulated in fibroblasts, and they stimulate the proliferation and differentiation of the keratinocytes [26, 67]. During the mid-phase of keratinocyte-fibroblast interactions, the balance of keratinocyte-derived IL-1 and TGF--β effects begins to shift. In fibroblasts, NF-κB activation is decreasing,

whereas TGF-β-dependent gene expression is increasing again. The fibroblasts begin to synthesize greater quantities of basement membrane components. In the later stage, TGF-β-dependent effects actions completely control the fibroblasts phenotype. Although mature keratinocyte-derived IL-1 is still detectable, the NF-kB activation in fibroblasts appears to only moderately impede TGF-β signaling. Basement membrane components are extensively expressed by fibroblasts and help create a well-organized basement membrane zone [68-70].

In this research, the 3D-SFnws/ES hybrid imitated the epithelial-mesenchymal structure of normal skin. The electrospun (ES) layer of SF nanofibers acts as a temporary cutaneous basement membrane. We expect that after implantation into the wound bed this ES layer will act as an attachment scaffold for keratinocytes to complete their necessary proliferation and metabolic tasks before its eventual degradation. Previously, once the ES silk fibroin scaffolds had been implanted *in vivo*, even though that most of these materials retained their structural integrity, the visible SF fiber fragmentation was evidence of their degradation, and the scaffolds were entirely degraded 8 weeks after implantation [71]. However, we only collected and extracted exosomes during the first 15 days of coculturing HDFs and HaCaT cells on

3D-SFnws/ES hybrids and in Transwell systems. Our findings can only partly reveal the keratinocyte-fibroblast interactions occurring in this microenvironment (SF fibers of 3D-SFnws/ES) at the early stage of wound healing.

Notably, among the IFs conveyed by the mixed exosomes released from two different cell types, the expression of interleukin-8 (IL-8) in the 3D-SFnws/ES hybrids group was increased *vs*. the Transwell group (control group). The endogenous IL-8 plays a role in all the phases of human wound healing, and keratinocyte-produced IL-8 is crucial for attracting neutrophils in the early stages of it [72, 73]. The expression of interleukin-10 (IL-10) is also significantly higher in the 3D-SFnws/ES hybrids group than cells in the Transwell system exosomes. IL-10 plays an important regulatory role in the early stage, which is the phase of specific infiltration with neutrophils and macrophages, as well as in the inflammatory response of cutaneous wound healing [74]. In addition, eosinophil chemotactic protein 2 (Eotaxin-2) also known as Chemokine (C-C motif) ligand 24 (CCL24), induces chemotaxis in eosinophils, and is also strongly chemotactic for resting T lymphocytes and slightly chemotactic for neutrophils [75, 76]. The expression of Eotaxin-2 also was significantly increased in 3D-SFnws/ES hybrids group. And similarly to the AGFs antibody

array test, MCP-1 expression was also significantly higher in the 3D-SFnws/ES hybrids group than the Transwell group exosomes(Figure 5, Table 2)

The above results show that HDFs and HaCaT cells co-grown in 3D-SFnws/ES hybrids release exosomes carrying enriched amounts of cytokines and chemokines regulating the inflammatory response at the early stage of Keratinocyte-Fibroblast Interactions.

Macrophage accumulation following tissue damage is no longer seen as merely a proxy for disease severity since macrophages are now understood to play a critical role in tissue regeneration in a variety of circumstances [77]. Depending on the way they are activated, macrophages have been broadly classified into two groups： M1 macrophages that are associated with pro-inflammatory outcomes and M2 macrophages that promote a more reparative upshot [78, 79].

Macrophage Inflammatory Proteins-1α (MIP-1α) is one of the only two forms (MIP-1α and MIP-1β) of MIPs in human beings [80]. They are major factors produced by macrophages and monocytes after stimulated with bacterial endotoxin or proinflammatory cytokines such as IL-1. However, MIPs can also be produced by some tissue cells, such as fibroblasts, epithelial cells and vascular smooth muscle cells [81]. They are crucial for immune responses in

inflammatory contexts [82]. Their main effect is pro-inflammatory and mainly consists in the activation of chemotaxis and migration, but also of bioactive molecules release. These chemokines molecules MIPs affect monocytes, T lymphocytes, dendritic cells, NK cells, and platelets. They also induce the synthesis and release of other pro-inflammatory cytokines such as IL-1, IL-6 and TNF-α from fibroblasts and macrophages [81]. The macrophage colony-stimulating factor (M-CSF), also known as colony stimulating factor 1 (CSF1), is associated with M2 macrophages polarization [83, 84]. Conversely, macrophages responding to granulocyte-macrophage colony-stimulating factor (GM-CSF) exhibit M1-associated phenotypic characteristics [85, 86]. Relevant lines of evidence show that during tissue injury and repair there exists a balance between M-CSF and GM-CSF mediated anti-inflammatory and pro-inflammatory activity. When the ratio tips toward M-CSF, the balance shifts to the M-CSF-mediated reparative/homeostatic state [83, 87]. So the significantly higher expression of M-CSF in exosomes released from HDFs and HaCaT cells cocultured on 3D-SFnws/ES hybrids suggests that this novel SF scaffold can promote the shift of macrophages toward the M2 phenotype which is reparative and anti-inflammatory. Even the expression of MIP-1α significantly increased in the exosomes

released from the 3D-SFnws/ES hybrids group (Figure 5; Table 2).

Conclusions

By combining a layer of electrospun SF nanofibers with the original 3D-SFnws scaffolds, we obtained the novel 3D-SFnws/ES hybrid scaffold with stable physical and chemical properties. Its special double-sided 3D structure successfully imitated the epithelial-mesenchymal structure of normal skin. And HDFs and HaCaT cells could adhere and proliferate well on 3D-SFnws side and electrospun side, respectively. The present results show that HDFs and HaCaT cells co-grown on these novel 3D-SFnws/ES hybrids release exosomes which convey significant amounts of AGFs and intensely stimulate HDMVECs to form endothelial tubes *in vitro*. These findings prove that the new improved SF scaffold based on the previous 3D-SFnws still retains some of their original excellent features, which are the promotion of angiogenesis and positive regulation of ECM remodeling. Furthermore, the exosomes released from HDFs and HaCaT cells cocultured on it also include various IFs which can promote and orderly regulate inflammatory responses by mediating keratinocyte-fibroblast interactions at the early stage of wound healing. These preliminary findings gained from the novel 3D-SFnws/ES hybrids are well worthy of further studies aimed at their potential application as a tissue engineering

dermal scaffold promoting for wounds (e.g. burns, traumas, diabetic ulcers, scar excision, and other kinds of wounding agent) healing in clinical settings.

Acknowledgements

I gratefully acknowledge I had received the fellowship from the INVITE project by the European Union's Horizon 2020 Research and Innovation Programme under the Marie Sklodowska-Curie Grant Agreement NO. 754345.

I gratefully acknowledge Dr. Giuliano Freddi (Silk Biomaterials, Como, Italy) for his essential contribution to the preparation and chemico-physycal analysis of the 3D-SFnws/ES-hybrid scaffolds.

References

1. Singer AJ, Clark RAF. Cutaneous wound healing. N Engl J Med. 1999; 341(10): 738–746.
2. Vincent Gabriel. Hypertrophic scar. Phys Med Rehabil Clin N Am. 2011; 22(2):301-10.
3. Matsumura H, Imai R, Ahmatjan N, et al. Removal of adhesive wound dressing and its effects on the stratum corneum of the skin: comparison of eight different adhesive wound dressings. Int Wound J. 2014; 11(1):50-54.
4. Leung A, Crombleholme TM, Keswani SG. Fetal wound healing: implications for minimal scar formation. Curr Opin Pediatr. 2012; 24(3):371-378.
5. Hu DH, Zhang ZF, Zhang YG, et al. A potential skin substitute constructed with hEGF gene modified HaCaT cells for treatment of burn wounds in a rat model. Burns. 2012; 38(5):702-712.
6. Song G, Wu Y, Wang F, et al. Development and preparation of a lowimmunogenicity porcine dermal scaffold and its biocompatibility assessment. J Mater Sci Mater Med. 2015; 26(4):170.
7. Haejun Yim, Yong Suk Cho, et al. The use of AlloDerm on major burn patients: AlloDerm prevents post-burn joint contracture. Burns. 2010; 36(3):322-328.

8. M Ayaz, A Najafi, et al. Thin Split Thickness Skin Grafting on Human Acellular Dermal Matrix Scaffold for the Treatment of Deep Burn Wounds. Int J Org Transplant Med. 2021; 12 (1): 44-50.
9. Klosová H, Klein L, Bláha J. Analysis of a retrospective doublecentre data-collection for the treatment of burns using biological cover Xe-derma®. Ann Burn Fire Disasters. 2014; 27(4): 171-175.
10. Abraham LM. Xenaderm: an essential wound care therapy. Adv Skin Wound Care. 2010; 23(2): 73-76.
11. Taghiabadi E, Nasri S, Shafieyan S, et al. Fabrication and characterization of spongy denuded amniotic membrane based scaffold for tissue engineering. Cell J. 2015; 16(4):476-487.
12. Mondal M. The silk proteins, sericin and fibroin in silkworm, Bombyx mori Linn.,-a review. Caspian Journal of Environmental Sciences. 2007; 5(2): 63-76
13. Kundu B, Rajkhowa R, Kundu S C, et al. Silk fibroin biomaterials for tissue regenerations. Adv Drug Deliv Rev. 2013; 65(4): 457-470.
14. Kim I Y, Seo S J, Moon H S, et al. Chitosan and its derivatives for tissue engineering applications. Biotechnol Adv. 2008; 26(1): 1-21.
15. Sanzana ES, Navarro M, Ginebra MP, et al. Role of porosity and pore architecture in the in vivo bone regeneration capacity of biodegradable glass scaffolds. Biomed Mater Res A. 2014; 102(6): 1767-1773.

16. Heard A J, Socrate S, Burke K A, et al. Silk-based injectable biomaterial as an alternative to cervical cerclage: an in vitro study. Reproductive Sciences. 2013; 20(8): 929-936.
17. Elliott W H, Bonani W, Maniglio D, et al. Silk hydrogels of tunable structure and viscoelastic properties using different chronological orders of genipin and physical cross-linking. ACS applied materials & interfaces. 2015; 7(22): 12099-12108.
18. Hodgkinson T, Yuan XF. Electrospun silk fibroin fiber diameter influences in vitro dermal fibroblast behavior and promotes healing of ex vivo wound models. J Tissue Eng. 2014; 5:eCollection 2014.
19. Wei Zhang, Longkun Chen, et al. Silk Fibroin Biomaterial Shows Safe and Effective Wound Healing in Animal Models and a Randomized Controlled Clinical Trial. Adv Healthc Mater. 2017; 6(10). Epub 2017 Mar 24.
20. Dimple Chouhan, Bijayshree Chakraborty, et al. Role of non-mulberry silk fibroin in deposition and regulation of extracellular matrix towards accelerated wound healing. Acta Biomater. 2017; 48:157-174.
21. Keller S, Sanderson MP, Stoeck A, Altevogt P. Exosomes: from biogenesis and secretion to biological function. Immunol Lett. November 2006; 107(2):102–108.
22. Booth AM, Fang Y, Fallon JK, Yang JM, Hildreth JE, Gould SJ.

Exosomes and HIV gag bud from endosome-like domains of the T cell plasma membrane. J Cell Biol. March 2006; 172(6):923–935.

23. Simons M, Raposo G. Exosomes-vesicular carriers for intercellular communication. Curr Opin Cell Biol. 2009; 21(4):575–581.
24. van der Pol E, Böing AN, Harrison P, Sturk A, Nieuwland R. Classification, functions, and clinical relevance of extracellular vesicles. Pharmacol Rev. July 2012; 64(3):676–705.
25. Tkach M, Thery C. Communication by extracellular vesicles:where we are and where we need to go. Cell. 2016; 164(6):1226–1232.
26. Sabine Werner, Thomas Krieg, et al. Keratinocyte-fibroblast interactions in wound healing. J Invest Dermatol. 2007 ; 127(5):998-1008.
27. Melanie Gartz, Jennifer L Strande. Examining the Paracrine Effects of Exosomes in Cardiovascular Disease and Repair. J Am Heart Assoc. 2018; 7(11):e007954.
28. Joshua L Hood, Hua Pan,et al. Paracrine induction of endothelium by tumor exosomes. Lab Invest. 2009; 89(11):1317-1328.
29. Samantha Sheller-Miller, Jayshil Trivedi, et al. Exosomes Cause Preterm Birth in Mice: Evidence for Paracrine Signaling in Pregnancy.Sci Rep. 2019; 9(1):608.
30. Lai R C, Arslan F, Lee M M, et al. Exosome secreted by MSC reduces myocardial ischemia/reperfusion injury. Stem Cell Res, 2010; 4(3):

214-222.

31. Peng Hu, Qinxin Yang, et al. Mesenchymal stromal cells-exosomes: a promising cell-free therapeutic tool for wound healing and cutaneous regeneration. Burns Trauma. 2019; 7:38.
32. Ali Golchin,Simzar Hosseinzadehet al. The exosomes released from different cell types and their effects in wound healing. J Cell Biochem. 2018; 119(7):5043-5052.
33. Dal Prà I, Freddi G, et al. De novo engineering of reticular connective tissue in vivo by silk fibroin nonwoven materials. Biomaterials. 2005; 26:1987–1999.
34. Dal Prà I, Chiarini A, et al. Novel dermo-epidermal equivalents on silk fibroin-based formic acidcrosslinked three-dimensional nonwoven devices with prospective applications in human tissue engineering/regeneration/repair. Int J Mol Med. 2006; 18:241–247.
35. Chiarini A, Freddi G, et al. Biocompatible silk noil-based three-dimensional carded-needled nonwoven scaffolds guide the engineering o novel skin connective tissue. Tissue Eng Part A. 2016; 22:1047–1060.
36. Peng Hu, Anna Chiarini, et al. Exosomes of adult human fibroblasts cultured on 3D silk fibroin nonwovens intensely stimulate neoangiogenesis. Burns Trauma. 2021; 9:tkab003.
37. P Boukamp, R T Petrussevska, et.al. Normal keratinization in a

spontaneously immortalized aneuploid human keratinocyte cell line. J Cell Biol. 1988; 106(3):761-771.

38. B Marelli, A Alessandrino, et.al. Compliant electrospun silk fibroin tubes for small vessel bypass grafting, Acta Biomater., 2010; 6, 4019-4026.
39. A Alessandrino. Process for the production of a hybrid structure consisting of coupled silk fibroin microfibers and nanofibers, hybrid structure thus obtained and its use as implantable medical device, 2016, WO 2016/067189A1.
40. Chiarini A, Armato U, et al. Amyloid β- exposed human astrocytes overproduce Phospho-tau and Overrelease it within exosomes, effects suppressed by Calcilytic NPS 2143-further implications for Alzheimer's therapy.Front Neurosci. 2017; 11:217.
41. Patel GK, Khan MA, et al. Comparative analysis of exosome isolation methods using culture supernatant for optimum yield, purity and downstream applications. Sci Rep. 2019; 9(1):5335.
42. Nakamura K, Jinnin M, et al. Altered expression of CD63 and exosomes in scleroderma dermal fibroblasts. J Dermatol Sci. 2016; 84: 30-39.
43. Joanna Kowal, Mercedes Tkach, et al. Biogenesis and secretion of exosomes. Curr Opin Cell Biol. 2014 Aug;29:116-125.
44. Zhang K, Mo X, et al. Electrospun scaffolds from silk fibroin and

their cellular compatibility. J Biomed Mater Res A. 2010; 93:976–983.

45. Lotz B, Colonna Cesari F. The chemical structure and the crystalline structures of Bombyx mori silk fibroin. Biochimie. 1979; 61:205.
46. Huang R, Jiang W, et al. A biotin label-based antibody array for high-content profiling of protein expression. Cancer Genomics Proteomics. 2010; 7:129-141.
47. Michael Blair, Jake D Jones, et al. Skin Structure-Function Relationships and the Wound Healing Response to Intrinsic Aging. Adv Wound Care (New Rochelle). 2020; 9(3):127-143.
48. Zeeuwen PL. Epidermal differentiation: The role of proteases and their inhibitors . Eur J Cell Biol 2004 ; 83 : 761-773 .
49. Hachem J P , Man M Q , et al. Sustained serine proteases activity by prolonged increase in pH leads to degradation of lipid processing enzymes and profound alterations of barrier function and stratum corneum integrity . J Invest Dermatol. 2005; 125 : 510-520 .
50. Moser B, Clark-Lewis I, et al. Neutrophil-activating properties of the melanoma growth-stimulatory activity. The Journal of Experimental Medicine. 1990; 171 (5): 1797-1802.
51. Schumacher C, Clark-Lewis I, et al. High-and low-affinity binding of GRO alpha and neutrophil-activating peptide 2 to interleukin 8 receptors on human neutrophils. Proceedings of the National

Academy of Sciences of the United States of America. 1992; 89 (21): 10542-10546.

52. Engelhardt E, Toksoy A, et al. Chemokines IL-8, GRO alpha, MCP-1, IP-10, and Mig are sequentially and differentially expressed during phasespecific infiltration of leukocyte subsets in human wound healing. Am J Pathol. 1998; 153:1849-1860.
53. Christopherson K III, Hromas R. Chemokine regulation of normal and pathologic immune responses. Stem Cells. 2001; 19:388-396.
54. Girbl T, Lenn T, et al. Distinct compartmentalization of the chemokines CXCL1 and CXCL2 and the atypical receptor ACKR1 determine discrete stages of neutrophil diapedesis. Immunity. 2018; 49:1062, e6-76.
55. Carr MW, Roth SJ, et al. Monocyte chemoattractant protein 1 acts as a T-lymphocyte chemoattractant. Proceedings of the National Academy of Sciences of the United States of America. 1994; 91(9): 3652-3656.
56. Xu LL, Warren MK, et al. Human recombinant monocyte chemotactic protein and other C-C chemokines bind and induce directional migration of dendritic cells in vitro. Journal of Leukocyte Biology. 1996; 60 (3): 365-371.
57. Yuko Ishida, Yumi Kuninaka, et al. CCL2-Mediated Reversal of Impaired Skin Wound Healing in Diabetic Mice by Normalization of

Neovascularization and Collagen Accumulation. J Invest Dermatol. 2019; 139(12): 2517-2527.

58. Anisyah Ridiandries, Joanne T M Tan, et al. The Role of Chemokines in Wound Healing. Int J Mol Sci. 2018; 19(10):3217.
59. Mohan R, Chintala SK, et al. Matrix metalloproteinase gelatinase B (MMP-9) coordinates and effects epithelial regeneration. The Journal of Biological Chemistry. 2002; 277 (3): 2065-2072.
60. Kobayashi T, Kim H, et al. Matrix metalloproteinase-9 activates TGF-β and stimulates fibroblast contraction of collagen gels. American Journal of Physiology. Lung Cellular and Molecular Physiology. 2014; 306 (11): 1006-1015.
61. TIMP2 TIMP metallopeptidase inhibitor 2 [Homo sapiens (human)]. Gene ID: 7077, updated on 28-Nov-2021.
62. Bourboulia D, Stetler-Stevenson WG. Matrix metalloproteinases (MMPs) and tissue inhibitors of metalloproteinases (TIMPs): Positive and negative regulators in tumor cell adhesion. Seminars in Cancer Biology. 2010; 20 (3): 161-168.
63. Vaalamo M, Leivo T, et al. Differential expression of tissue inhibitors of metalloproteinases (TIMP-1, −2, −3, and −4) in normal and aberrant wound healing. Hum Pathol. 1999; 30:795-802.
64. N Maas-Szabowski, A Shimotoyodome, et al. Keratinocyte growth regulation in fibroblast cocultures via a double paracrine mechanism.

J Cell Sci. 1999; 112 (Pt 12):1843-1853.

65. D T Graves, N Nooh, et al. IL-1 plays a critical role in oral, but not dermal, wound healing. J Immunol. 2001; 167(9):5316-5320.
66. Han Chung Chong, Ming Jie Tan, et al. Regulation of epithelial-mesenchymal IL-1 signaling by PPARbeta/delta is essential for skin homeostasis and wound healing. J Cell Biol. 2009; 184(6):817-831.
67. Yuko Ishida, Toshikazu Kondo, et al. Absence of IL-1 receptor antagonist impaired wound healing along with aberrant NF-kappaB activation and a reciprocal suppression of TGF-beta signal pathway. J Immunol. 2006; 176(9):5598-5606.
68. Pierre Shephard, Boris Hinz, et al. Dissecting the roles of endothelin, TGF-beta and GM-CSF on myofibroblast differentiation by keratinocytes. Thromb Haemost. 2004; 92(2):262-274.
69. R P Nagarajan, F Chen, et al. Repression of transforming-growth-factor-beta -mediated transcription by nuclear factor kappaB. Biochem J. 2000; 348 Pt 3(Pt 3):591-596.
70. Diana V Messadi, Hai S Doung, et al. Activation of NFkappaB signal pathways in keloid fibroblasts. Arch Dermatol Res. 2004; 296(3):125-133.
71. Juan Zhou, Chuanbao CaoIn, et al. vitro and in vivo degradation behavior of aqueous-derived electrospun silk fifibroin scaffolds.

Polymer Degradation and Stability. 2010; 95 : 1679-1685.

72. H O Rennekampff, J F Hansbrough, et al. Bioactive interleukin-8 is expressed in wounds and enhances wound healing. J Surg Res. 2000; 93(1):41-54.
73. Cheng-Che E Lan, Ching-Shuang Wu, et al. High-glucose environment enhanced oxidative stress and increased interleukin-8 secretion from keratinocytes: new insights into impaired diabetic wound healing. Diabetes. 2013; 62(7):2530-2358.
74. Y Sato, T Ohshima, et al. Regulatory role of endogenous interleukin-10 in cutaneous inflammatory response of murine wound healing. Biochem Biophys Res Commun. 1999; 265(1):194-199.
75. V P Patel, B L Kreider, et al. Molecular and functional characterization of two novel human C-C chemokines as inhibitors of two distinct classes of myeloid progenitors. J Exp Med, 1997; 185(7):1163-1172.
76. J R White, C Imburgia, et al. Cloning and functional characterization of a novel human CC chemokine that binds to the CCR3 receptor and activates human eosinophil. J Leukoc Biol. 1997; 62(5):667-675.
77. Christina V Jones, Sharon D Ricardo. Macrophages and CSF-1: implications for development and beyond. Organogenesis. 2013; 9(4):249-260.
78. Alberto Mantovani, Antonio Sica, et al. The chemokine system in

diverse forms of macrophage activation and polarization. Trends Immunol. 2004; 25(12):677-686.

79. Fernando Oneissi Martinez, Antonio Sica, et al. Macrophage activation and polarization. Front Biosci. 2008; 13:453-461.
80. A Zlotnik, O Yoshie. Chemokines: a new classification system and their role in immunity. Immunity. 2000; 12(2):121-127.
81. Menten P, Wuyts A, et al. Macrophage inflammatory protein-1. Cytokine & Growth Factor Reviews. 2002; 13 (6): 455-481.
82. Min Ren, Qing Guo, et al. Polymerization of MIP-1 chemokine (CCL3 and CCL4) and clearance of MIP-1 by insulin-degrading enzyme. EMBO J. 2010; 29(23):3952-3966.
83. John A Hamilton. Colony-stimulating factors in inflammation and autoimmunity. Nat Rev Immunol. 2008; 8(7):533-544.
84. Svensson J, Jenmalm MC, et al. Macrophages at the fetal-maternal interface express markers of alternative activation and are induced by M-CSF and IL-10. J Immunol. 2011; 187(7):3671-3682.
85. Frank A W Verreck, Tjitske de Boer, et al. Human IL-23-producing type 1 macrophages promote but IL-10-producing type 2 macrophages subvert immunity to (myco)bacteria. Proc Natl Acad Sci U S A. 2004; 101(13): 4560-4565.
86. Andrew J Fleetwood, Toby Lawrence, et al. Granulocyte-macrophage colony-stimulating factor (CSF) and macrophage CSF-dependent

macrophage phenotypes display differences in cytokine profiles and transcription factor activities: implications for CSF blockade in inflammation. J Immunol. 2007;178(8):5245-5252.

87. John A Hamilton. Colony stimulating factors and macrophage heterogeneity. Inflammation and Regeneration. 2011; 31(3): 228-236.